การสังเคราะห์ด้วยกระบวนการทางไฟฟ้าเคมีอย่างมีประสิทธิภาพและเลือกสรรของ 4-อะมิโนฟีนอล ในสภาวะพีเอชเป็นกลางด้วยขั้วไฟฟ้าชนิดนิกเกิล-เหล็ก-ฟอสไฟต์

EFFICIENT AND SELECTIVE ELECTROSYNTHESIS OF 4-AMINOPHENOL AT NEUTRAL PH BASED ON NICKEL-IRON PHOSPHIDE MODIFIED ELECTRODE

ปพนธีร์ แซ่อ๋อง

PAPONTEE SAE ONG

วิทยานิพนธ์นี้เป็นส่วนหนึ่งของการศึกษาตามหลักสูตรปริญญาวิศวกรรมศาสตรมหาบัณฑิต

สาขาวิชาวิศวกรรมเคมี

คณะวิศวกรรมศาสตร์

สถาบันเทคโนโลยีพระจอมเกล้าเจ้าคุณทหารลาดกระบัง

พ.ศ. 2566

KMITL-2023-EN-M-220-176

EFFICIENT AND SELECTIVE ELECTROSYNTHESIS OF 4-AMINOPHENOL AT NEUTRAL PH BASED ON NICKEL-IRON PHOSPHIDE MODIFIED ELECTRODE

PAPONTEE SEA ONG

A THESIS SUBMITTED IN PARTIAL FULFILLMENT
OF THE REQUIREMENTS FOR THE DEGREE OF
MASTER OF ENGINEERING IN CHEMICAL ENGINEERING
SCHOOL OF ENGINEERING
KING MONGKUT'S INSTITUTE OF TECHNOLOGY LADKRABANG
2023

KMITL-2023-EN-M-220-176

THESIS STATEMENT

This work is based on a published article: Papontee Sae Ong, Shih-Ching Huang, Chia-Yu Lin, Nuttapol Lerkkasemsan, "**Efficient and selective electrosynthesis of 4-aminophenol at circumneutral pH from the electrocatalytic reduction of nitrophenol over the nickel-iron phosphide modified electrode"**, Materials Today Sustainability, Volume 24, 2023, 100547, ISSN 2589-2347, doi: 10.1016/j.mtsust.2023.100547.

Thesis	Efficient and Selective Electrosynthesis of 4-Aminophenol at Neutral pH Based on Nickel-Iron Phosphide Modified Electrode
Student	Papontee Sae Ong
Student ID.	63601053
Degree	Mater of Engineering
Program	Chemical Engineering
Year	2023
Thesis Advisor	Asst. Prof. Dr. Nuttapol Lerkkasemsan (KMITL, Thailand)
Thesis Number	KMITL-2023-EN-M-220-176

ABSTRACT

The energy and pollution dilemma has emerged as a significant worldwide issue and source of worry in recent years. Electrochemical reduction with water as the hydrogen donor source serves as a sustainable synthetic alternative route for green electrochemical synthesis without the use of hazardous and expensive reagents. Specifically, efficient and selective electrosynthesis of 4-aminophenol via electrochemical reduction of 4-nitrophenol (*e*-NPR) can be achieved at potentials lower than those of the hydrogen evolution reaction. Herein, this study represents the facile electrochemical synthesis of micro-structured nickel-iron phosphide on carbon paper (*micro*NiFeP|CP) with high activity in catalyzing *e*-NPR at neutral pH. A series of controlled-potential electrolyses (CPEs) were utilized to thoroughly examine the electrolysis conditions, including the electrolyte pH, applied potential, and electrolysis duration, on the electrosynthesis of 4-AP. Under optimal conditions, the optimized *micro*NiFeP|CP (*micro*NiFeP|CP*op*) electrode exhibited *e*-NPR onset at 0.13 V vs. RHE. The *micro*NiFeP|CP*op* electrode had a turnover rate of 7.25 ± 0.05 h^{-1} to generate 4-AP at 0.0 V vs. RHE. Moreover, it also had a high 4-NP conversion rate of 92.29 ± 1.47% and a high selectivity (85.77 ± 2.21%) to generate 4-AP after 8 hours of CPEs at -0.15 V vs. RHE, which generated 4-AP at a rate of 25.45 ± 1.73 μmole cm^{-2} h^{-1} in the H-cell. In addition, the scale-up electrosynthesis of 4-AP with a flow-type electrolyzer was also demonstrated. The 3-h electrolysis using the flow-type electrolyzer operation at -10 mA cm^{-2} resulted in a high 4-NP conversion (93.84 ± 0.84%) with a high S_{AP} (86.32 ± 1.05%). Finally, the probable reaction pathways of *e*-

NPR have been proposed, and the main side products have been identified as 4,4'-dihydroxyazobenzene and dimers.

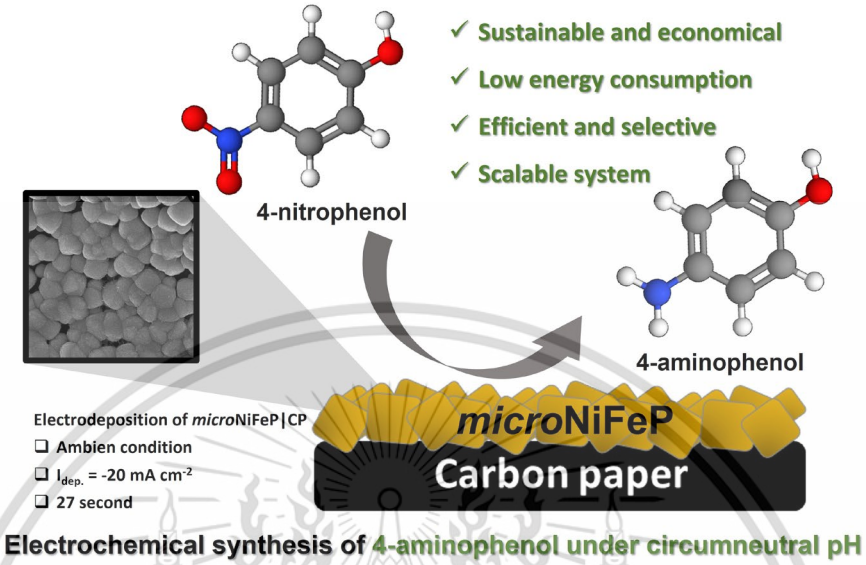

Key words: Electrochemical reduction, Nickel-iron phosphide electrode, 4-Aminophenol, 4-Nitrophenol, Flow-type electrolyzer

หัวข้อวิทยานิพนธ์	การสังเคราะห์ด้วยกระบวนการทางไฟฟ้าเคมีอย่างมีประสิทธิภาพและเลือกสรรของ 4-อะมิโนฟีนอล ในสภาวะพีเอชเป็นกลางด้วยขั้วไฟฟ้าชนิดนิกเกิล-เหล็ก-ฟอสไฟต์
นักศึกษา	นายปพนธีร์ แซ่อ๋อง
รหัสประจำตัว	63601053
ปริญญา	วิศวกรรมศาสตรมหาบัณฑิต
สาขาวิชา	วิศวกรรมเคมี
พ.ศ.	2566
อาจารย์ที่ปรึกษาวิทยานิพนธ์	ผศ. ดร. ณัฐพล ฤกษ์เกษมสันต์ (สจล.)
หมายเลขวิทยานิพนธ์	KMITL-2023-EN-M-220-176

บทคัดย่อ

เนื่องด้วยในปัจจุบันปัญหาด้านพลังงานและมลพิษทางด้านสิ่งแวดล้อมกำลังเป็นที่สนใจ งานวิจัยฉบับนี้เล่งเห็นถึงปัญญาเหล่านี้จึงทำการศึกษาและพัฒนากระบวนการสังเคราะห์ 4-อะมิโนฟีนอล (4-aminophenol; 4-AP) ที่มีประสิทธิภาพและยั่งยืนผ่านปฏิกิริยารีดักชันด้วยกระบวนการทางไฟฟ้าเคมีของ 4-ไนโตรฟีนอล (electrochemical reduction of 4-nitrophenol; *e*-NPR) โดยใช้โปรตอน (proton) ที่ได้จากกระบวนการทางไฟฟ้าเคมีของน้ำด้วยตัวเร่งปฏิกิริยาทางไฟฟ้าเคมีที่ผ่านการพัฒนา ที่สามารถเพิ่มประสิทธิภาพในจลนศาสตร์ของปฏิกิริยารีดักชันด้วยกระบวนการทางไฟฟ้าเคมีของ 4-ไนโตรฟีนอลและการเลือกสรรของ 4-อะมิโนฟีนอลในสภาวะที่ไม่เป็นอันตรายต่อสิ่งแวดล้อม ในการศึกษานี้รายงานเกี่ยวกับการสังเคราะห์ด้วยกระบวนการทางไฟฟ้าเคมีที่มีประสิทธิภาพและยั่งยืนของ 4-อะมิโนฟีนอลที่พีเอชเป็นกลาง (pH 7) โดยใช้ขั้วไฟฟ้าชนิดนิกเกิล-เหล็ก-ฟอสไฟต์ที่มีโครงสร้างระดับจุลภาค (*micro*NiFeP|CP) ปัจจัยที่ส่งผลต่อการสังเคราะห์ด้วยกระบวนการทางไฟฟ้าเคมีของ 4-อะมิโนฟีนอลได้รับการตรวจสอบอย่างละเอียดผ่านการแยกสลายด้วยกระบวนการทางไฟฟ้าเคมีแบบควบคุมศักย์ (controlled-potential electrolysis, CPE) ภายใต้สภาวะที่เหมาะสม อันประกอบด้วย อัตราส่วนของนิกเกิลและเหล็กบนขั้วไฟฟ้าชนิดนิกเกิล-เหล็ก-ฟอสไฟต์ที่มีโครงสร้างระดับจุลภาคและสภาะในการแยกสลายด้วยกระบวนการทางไฟฟ้าเคมี (electrolysis) อาธิ ค่า pH ของอิเล็กโทรไลต์ ศักย์ไฟฟ้าที่ใช้ และระยะเวลาในกระบวนการขั้วไฟฟ้าชนิดนิกเกิล-เหล็ก-ฟอสไฟต์ที่มีโครงสร้างระดับจุลภาคที่ผ่านการพัฒนาแสดงประสิทธิภาพของตัวเร่งปฏิกิริยาทำได้โดยตรงจากค่าความถี่ผันเวียน (turnover frequency; TOF) ที่ 7.25 ± 0.05 ต่อชั่วโมง สำหรับการสังเคราะห์ 4-อะมิโนฟีนอลที่ศักย์ 0.0 โวลต์ (V vs. RHE) และการเปลี่ยนของ 4-ไนโตรฟีนอลสูงถึง 92.29 ± 1.47% โดยมีความสามารถในการเลือกสรรของ 4-อะมิโนฟีนอลสูงถึง 85.77 ± 2.21% ที่ศักย์ -0.15 โวลต์ (V vs. RHE) หลังจากทำการแยกสลายด้วยกระบวนการ

ทางไฟฟ้าเคมีแบบควบคุมศักย์เป็นเวลา 8 ชั่วโมง ซึ่งมีอัตราในการสังเคราะห์ 4-อะมิโนฟีนอลถึง 25.45 ± 1.73 ไมโครโมลต่อตารางเซนติเมตรต่อชั่วโมง ในเครื่องแยกสลายด้วยกระบวนการทางไฟฟ้าเคมีแบบ 2 ส่วน (H-cell-type electrolyzer; two-compartment electrolyzer) นอกจากนี้ การสังเคราะห์ด้วยกระบวนการทางไฟฟ้าเคมีของ 4-อะมิโนฟีนอลด้วยเครื่องแยกสลายด้วยกระบวนการทางไฟฟ้าเคมีแบบไหล (flow-type electrolyzer) อีกด้วยการแยกสลายด้วยไฟฟ้าเป็นเวลา 3 ชั่วโมง โดยใช้เครื่องแยกสลายด้วยกระบวนการทางไฟฟ้าเคมีแบบไหลที่มีการความคุมกระแสคงที่ที่ -10 มิลลิแอมป์ต่อตารางเซนติเมตร ให้ประสิทธิภาพในการเปลี่ยน 4-ไนโตรฟีนอลสูงถึง 93.84 ± 0.84% โดยมีการเลือกสรรของ 4-อะมิโนฟีนอลสูงถึง 86.32 ± 1.05% นอกจากนี้ มีการศึกษาเพิ่มเติมเกี่ยวกับเส้นทางการเกิดปฏิกิริยาที่เป็นไปได้ของปฏิกิริยารีดักชันด้วยกระบวนการทางไฟฟ้าเคมีของ 4-ไนโตรฟีนอลและผลิตภัณฑ์ข้างเคียงหลัก (by products) อาธิ 4,4'-ไดไฮดรอกซีอะโซเบนซีน (4,4’-dihydroxyazobenzene) และไดเมอร์ (dimers)

คำสำคัญ: ปฏิกิริยารีดักชันด้วยกระบวนการทางไฟฟ้าเคมี ขั้วไฟฟ้าชนิดนิกเกิล-เหล็ก-ฟอสฟอไฟต์ 4-ไนโตรฟีนอล 4-อะมิโนฟีนอล เครื่องแยกสลายด้วยกระบวนการทางไฟฟ้าเคมีแบบไหล

ACKNOWLEDGEMENTS

I would like to express my deepest appreciation to my advisors, Prof. Chia-Yu Lin (NCKU) and Asst. Prof. Dr. Nuttapol Lerkkasemsan (KMITL) who provided me with the opportunity to undertake an excellent electrochemical project. My advisor also supports me in the research and provides suggestions for guidelines. Without their guidance and persistent help, this thesis would not have been possible. Additionally, I am most grateful for the financial support from the National Science and Technology Council of Taiwan (110-2221-E-006-018-MY3 and 111-2221-E-006-019-MY3). This work was also financially supported by the Hierarchical Green-Energy Materials (Hi-GEM) Research Center from The Featured Areas Research Center Program within the framework of the Higher Education Sprout Project by the Ministry of Education (MOE) in Taiwan. I would also like to thank the use of ESCA003200 and XRD005100 belonging to the Core Facility Center of National Cheng Kung University.

I would like to express my deepest appreciation to all the committee members who were able to provide inspiration and suggestions to enrich the content of my thesis.

I would like to thank the laboratory members in ENSEN LAB (Prof. Chia-Yu Lin) and Artificial Photosynthesis LAB (Asst. Prof. Yi-Hsuan Lai) at NCKU for supporting and inspiring excellent ideas. Specifically, I am grateful to Shih-Ching Huang (as PhD candidate) and Ping-Chang Chuang (as PhD candidate) for their suggestions and support in a public paper and this research. Moreover, I would like to thank the laboratory members in Nuttapol's LAB at KMITL for supporting and inspiring excellent ideas. My research might not be successful without them.

Finally, I would like to thank the dual master's degree program of the cooperation between KMITL and NCKU, and I am most grateful to all professors in the school of engineering at King Mongkut's Institute of Technology Ladkrabang (KMITL) and the department of chemical engineering at National Cheng Kung University (NCKU) for providing the knowledge and experiences for the master's degree in chemical engineering.

Papontee Sae Ong

TABLE OF CONTENTS

LIST OF FIGURES

Page

LIST OF TABLES

Page

LIST OF SYMBOLS AND ABBREVIATIONS

4-NP	4-Nitrophenol
4-AP	4-Aminophenol
4-NSP	4-Nitrosophenol
*micro*NiFeP|CP	Modified microstructure nickel iron phosphide on carbon paper
*micro*FeP|CP	Modified microstructure iron phosphide on carbon paper
*micro*NiP|CP	Modified microstructure nickel phosphide on carbon paper
e-NPR	Electrochemical hydrogenation of 4-nitrophenol
(Photo)e-NPR	(Photo)-electrochemical hydrogenation of 4-nitrophenol
TMPs	Transition metal phosphides
DIW	Deionized water
CPEs	Controlled potential electrolysis
CCEs	Controlled current electrolysis
HER	Hydrogen evolution reaction
RHE	Reversible hydrogen electrode
PBS	Phosphate buffer solution
OCP	Open circuit potential
CV	Cyclic voltammetry
LSV	Linear sweep voltammogram
E	Potential (V)
S_{AP}	Selectivity of aminophenol (%)
N_i	Amount of i species (mole)
F	Faraday's constant ~ 96,485 C mol^{-1}
FE_i	Faradaic efficiency of i species (%)
TOF	Turnover of frequency (h^{-1})
k	kinetic rate constant (h^{-1} cm^{-1})
V	Volume of electrolyte (cm^3)
C_i	Concentration of i species (mM)
I, J	Current density (mA cm^{-2})
Q_i	Charge passage of i species (C; Coulomb)

Superscript and Subscript

NP	4-Nitrophenol
AP	4-Aminophenol
ΔNP	Partial difference of 4-nitrophenol
H2	Hydrogen gas
NiFe	Nickel to iron
hypophosphite	Hypophosphite
0	Initial
op	Optimized
dep	Electrodeposition

CHAPTER 1
INTRODUCTION

1.1 Background

Recently, water pollution caused by nitroaromatic compounds has become a critical concern. 4-nitrophenol (4-NP) is a key feedstock in the industrial production of pesticides, dyestuffs, herbicides, pharmaceuticals, etc. Nevertheless, 4-NP was designated as a priority hazardous pollutant by the United States Environmental Protection Agency (EPA) and Agency for Toxic Substances and Disease Registry (ATSDR) because of its high carcinogenicity and environmental persistence. Discharge of industrial effluents containing 4-NP to the environment after the above-mentioned industrial uses would pose a serious threat to human health and the environment [1]. To mitigate the 4-NP-related pollution, the development of cost-effective and eco-friendly approaches to removing 4-NP from industrial effluents before their discharge into the environment is of considerable relevance and urgency. Several methodologies to reduce the toxicity of 4-NP have been explored and developed, such as bioremediation [2], adsorption [3], catalytic reductive degradation [4, 5], (electro-)Fenton degradation [6], etc.

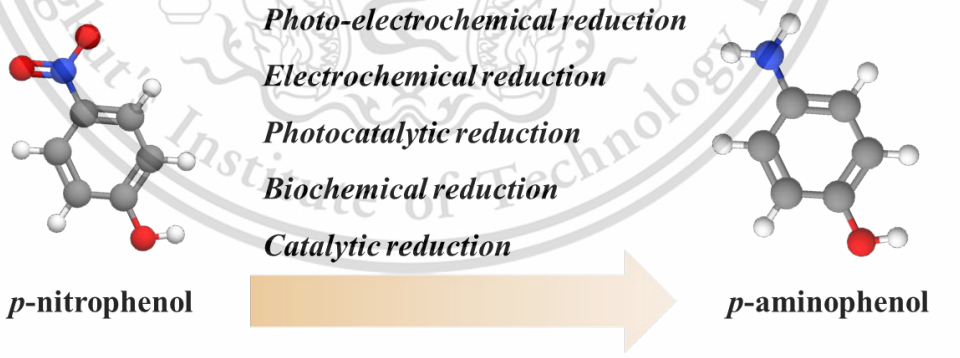

Figure 1-1 Scheme of remediation of 4-NP to generated 4-AP

The developed competitive of the remediation of 4-NP via electrochemical hydrogenation (*e*-NPR) serves as a cost-effective, environmentally benign, and sustainable approach as it provides several distinct advantages. First of all, *e*-NPR uses water as the hydrogen donor, which avoids the use of other hazardous and expensive

hydrogen donors, such as hydrazine and sodium borohydride, in the catalytic reductive degradation. Secondly, high current efficiency of ~99% can be achieved by *e*-NPR as compared with low current/electron efficiency of electro-Fenton degradation and catalytic reductive degradation. Notably, high removal rate of 4-NP by hydrazine and sodium borohydride in catalytic reductive degradation required the use of 100 times. Finally, *e*-NPR can be operated in the waste streams containing concentrated 4-NP with a wide pH range, whereas electro-Fenton and bioremediation methods suffer low efficiency at elevated 4-NP concentrations and solution pH values.

Previously, several electrocatalysts developed with precious noble metal-based cathode materials demonstrated effectiveness in catalyzing e-NPR with high conversion and selectivity under strongly alkaline [7] or acidic [8] conditions, whereas circumneutral conditions received little attention in the development of active and selective electrocatalysts [9]. However, the reactivity and selectivity toward the target products, such as azoxy-, azo-, and amino-aromatic compounds, can be significantly influenced by the pH of the electrolytes and the applied potentials during electrocatalysis [10]. 4-Aminophenol (4-AP), as one production of *e*-NPR, is a valuable intermediate feedstock used in industries such as photography, dyestuff, pharmaceuticals, and cosmetics; nevertheless, the instability of 4-AP to oxidation leads to the formation of various oxidation products of aromatic amines, depending on variety of factors including temperature, exposure to light, pH condition, and oxidizing agent [11-13]. Nevertheless, electrochemical hydrogenation to reduce the toxicity of 4-NP under strong acidic or alkaline conditions is neither cost-effective nor eco-friendly. Consequently, the development of effectiveness and selectivity toward 4-AP with low-cost electrocatalysts under close circumneutral pH is challenged.

Recently, there has been a significant amount of research on developing effective electrocatalysts based on earth-abundant elements like iron, nickel metal, and phosphide for electrochemical hydrogenation reactions [14], particularly under closely circumneutral pH [5, 15]. While these catalysts have shown promising results, the activity of Ni or Fe species in the electrochemical reduction of 4-nitrophenol (4-NP) was found to improve when used for electro-sensing based on cyclic voltammetric measurements [16-18]. The beneficial role of iron species in the reduction of 4-NP has been investigated to describe the kinetics mechanism and a rate law for the conversion of 4-NP to 4-AP [19]. According to previous work, the facile electrochemical deposition of *micro*NiFeP electrodes exhibited high *e*-NPR activity and selectivity

against HER; moreover, the findings suggest that incorporating Fe and P species has also been found to enhance the e-NPR activity [20].

The experimental results indicate that the desired conversion and Faradic efficiency (FE) were achieved, and the dominant product of *e*-NPR with *micro*NiFeP|CP electrodes was 4-AP; however, the selectivity of 4-AP synthesis is impacted by pH values and working potentials. Especially after 8 h-controlled-potential electrolysis (8 h-CPEs) at − 0.15 V vs. RHE in circumneutral pH, *micro*NiFeP|CP*op* achieved high conversion and selectivity. Therefore, the Earth-abundant elements-based electrocatalysts can be promising alternative catalyst for *e*-NPR. Moreover, the kinetics of e-NPR at circumneutral pHs to retrieve the mechanism underlying the electrosynthesis of 4-AP (e.g., the mode of e-/H+ transfer route) and established a *micro*NiFeP-based flow-type electrocatalytic platform for the efficient and selective electrosynthesis of 4-AP.

1.2 Motivations and Objectives

- To propose the beneficial roles of earth-abundant elements-based electrocatalysts as nickel, iron, and phosphorus in remediation toxicity-chemical (4-NP) to high-value products (4-AP).
- To challenge improved 4-NP electrochemical hydrogenation performance in neutral pH without pressurizing hydrogen and reducing agent/explosive hydrogen donors (e.g., $NaBH_4$).
- To propose the possible reaction pathway of *e*-NPR with *micro*NiFeP|CP and identify the side products.

1.3 Scopes of work

To promising alternative catalyst (as earth-abundant elements-based electrocatalysts), the investigation into the *e*-NPR using different molar ratios of nickel to iron in deposited electrolytes of *micro*NiFeP|CP and identified the active species of electrocatalytic toward *e*-NPR at neutral pH. Additionally, the operating conditions, including pH, working potential, reaction time, electrolyzer types, etc., were investigated.

CHAPTER 2
THEORY AND LITERATURE REVIEW

2.1 4-nitrophenol

4-Nitrophenol, also known as p-nitrophenol (4-NP), is a chemical compound with a yellow color and the molecular formula $C_6H_5NO_3$. It consists of a benzene ring with a nitro group ($-NO_2$) and a hydroxyl group (-OH) attached to it. This compound is sparingly soluble in water but dissolves easily in organic solvents. It is commonly used as an intermediate in the production of dyes, pharmaceuticals, and pesticides [20, 21]. Additionally, 4-NP can act as a pH indicator, changing its color depending on the acidity or alkalinity of the solution [22, 23]. However, it is important to handle this compound with caution as it is toxic if ingested, inhaled, or absorbed through the skin. Prolonged exposure can cause irritation and more severe health effects [24].

From an environmental perspective, 4-NP is a concern due to its toxicity to aquatic organisms. If released into water bodies, it can have detrimental effects on ecosystems. Therefore, it is crucial to handle and dispose of this compound properly to prevent environmental contamination. As with any chemical, it is essential to follow safety guidelines and regulations when working with 4-NP to minimize the risk to human health and the environment [24].

2.1.1 Toxicity of 4-nitrophenol

4-NP is a toxic chemical compound known for its harmful effects on human health and the environment. Ingestion of this compound can cause acute toxicity with symptoms like nausea, vomiting, and abdominal pain, and long-term exposure may lead to more severe health issues, including liver and kidney damage. Inhalation of 4-NP vapor can irritate the respiratory tract, while skin contact can result in irritation and allergic reactions. Moreover, its toxicity extends to aquatic organisms, making it harmful to aquatic ecosystems if released into water bodies. Furthermore, 4-NP has been found to exhibit mutagenic properties and is considered a potential carcinogen, warranting caution in handling and using this chemical to mitigate its adverse effects on both human and environmental health [24].

2.1.2 Remediation toxicity of 4-nitrophenol

2.1.2.1 Degradation of 4-nitrophenol (NPD)

The oxidation of 4-Nitrophenol (4-NP) involves a variety of processes with the objective of decomposing or transforming 4-NP into compounds that are less hazardous. Chemical oxidation, utilizing powerful oxidizing agents such as potassium permanganate ($KMnO_4$), hydrogen peroxide (H_2O_2), ozone (O_3), or persulfate ions ($S_2O_8^{2-}$), constitutes one method. By stimulating oxidation reactions, these agents facilitate the breakdown of 4-NP's nitro group, resulting in the formation of less hazardous and more basic compounds. An additional efficacious approach is Advanced Oxidation Processes (AOPs), which make use of exceedingly reactive hydroxyl radicals (•OH) produced during the decomposition of ozone or hydrogen peroxide. When exposed to heat or ultraviolet light, AOPs oxidize 4-NP molecules efficiently, thereby facilitating their degradation. In addition, photocatalytic oxidation, which utilizes photocatalysts based on semiconductors such as titanium dioxide (TiO_2) or zinc oxide (ZnO) and is activated by light, converts 4-NP into less hazardous byproducts. The goal of these oxidation processes is to mitigate the environmental consequences of 4-NP pollution through the conversion of it into compounds that are harmless to the environment [25].

Biological oxidation provides an additional pathway for the degradation of 4-NP. Enzymatic reactions enable specific microorganisms or enzymes to biologically oxidize 4-NP into metabolites that are less deleterious. This mechanism of biological degradation, which takes place within particular organisms, aids in the decomposition of 4-NP in the environment. Various oxidation techniques, including chemical, advanced oxidation, photocatalytic, and biological, are utilized to mitigate the detrimental effects of 4-NP pollution in effluent treatment and environmental remediation. These techniques are of the utmost importance in mitigating the persistence of 4-NP and advancing environmental sustainability through its conversion into less toxic compounds [25].

It is important to note that the specific degradation pathway and rate of 4-NP can vary depending on factors such as pH, temperature, presence of other pollutants, and the specific environment or treatment system. Additionally, the degradation products resulting from these processes may have their own environmental and toxicological implications.

2.1.2.2 Reduction of 4-nitrophenol (NPR)

The reduction of 4-NP encompasses studies on chemical, biological, photocatalytic, and electrochemical reduction processes. Metal catalysts, including platinum, palladium, gold, and silver, have been explored for chemical reduction, while microbial enzymes and bioremediation strategies have been investigated for biological reduction. Photocatalysis utilizing semiconductors like titanium dioxide and zinc oxide, as well as electrochemical techniques, have also been studied. Overall, the literature provides insights into various mechanisms and strategies for efficiently reducing 4-NP, offering potential applications in environmental remediation and sustainable chemistry [19, 26].

The reduction of 4-NP is important in various applications, including the synthesis of pharmaceuticals, dyes, and other organic compounds. By employing these reduction methods, particularly chemical and catalytic reduction, 4-NP can be transformed into less toxic or more valuable derivatives, contributing to environmental remediation and industrial processes.

2.2 4-aminophenol

4-Aminophenol (4-AP), a chemical compound denoted by the molecular formula C_6H_7NO, is characterized by its appearance as white to light brown crystals or powder. Its solubility properties reveal slight solubility in water but demonstrate higher solubility in organic solvents like ethanol and ether [13]. Caution is essential when handling 4-AP due to its potential health hazards. Direct contact can lead to irritation of the skin, eyes, and respiratory system. Prolonged or repeated exposure to this compound can potentially cause more severe health effects. Thus, strict adherence to safety measures is imperative. This includes the utilization of proper protective equipment such as gloves, goggles, and lab coats, working in well-ventilated areas, and strictly following safety guidelines and regulations established for handling hazardous substances. Such precautionary measures are crucial for minimizing and mitigating risks associated with the handling and use of 4-AP [13].

However, 4-AP holds significance as a crucial reactant in numerous industries. The global production of 4-AP has witnessed a remarkable surge, reaching millions of tons each year. This significant growth trend persists due to an ever-increasing demand within the chemical industry, as illustrated in **Figure 2-1** [13].

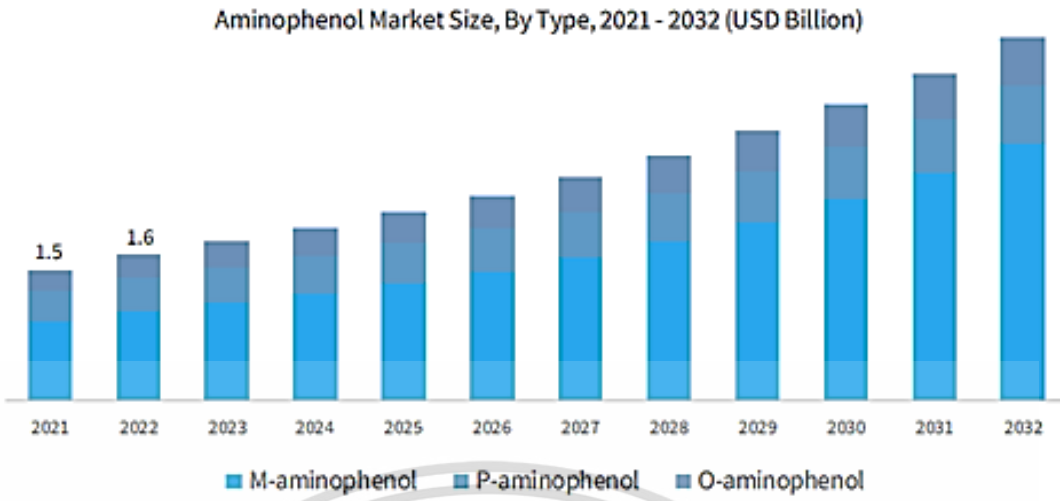

Figure 2-1 The global demand of 4AP [13]

2.2.1 Synthesis of 4-aminophenol

2.2.1.1 Chemical catalytic reduction of 4-nitrophenol

Chemical reduction with metal catalysts: platinum (Pt), palladium (Pd), gold (Au), and silver (Ag) have been used in a number of studies to work on the reduction of 4-NP. These catalysts can facilitate the transfer of electrons from a reducing agent to the nitro group, leading to its reduction. Various techniques, including heterogeneous catalysis and nanoparticle catalysts, have been employed to enhance the reduction efficiency [27].

2.2.1.2 Biological reduction of 4-nitrophenol

Biological reduction by microorganisms and enzymes: microbial reduction of 4-NP has been extensively investigated. Certain bacteria, fungi, and even enzymes produced by these microorganisms possess nitro-reductase enzymes that can catalyze the reduction reaction. Studies have identified and characterized specific strains of bacteria and fungi capable of efficiently reducing 4-nitrophenol. Bioremediation strategies utilizing these microorganisms have been explored for the treatment of contaminated environments [2].

2.2.1.3 Photoelectrochemical catalytic reduction and photochemical reduction of 4-nitrophenol

Photocatalytic reduction: photocatalysis, using semiconductor materials such as titanium dioxide (TiO_2) or zinc oxide (ZnO), has been investigated for the reduction of 4-NP. Under UV light irradiation, these photocatalysts generate electron-hole pairs that

can participate in the reduction reaction. This method offers a sustainable and environmentally friendly approach for 4-NP reduction [28].

2.2.1.4 Electrochemical catalytic reduction of 4-nitrophenol (e-NPR)

Electrochemical reduction: Electrochemical techniques, including direct electron transfer or mediated electron transfer, have been employed for the reduction of 4-NP. Electrochemical reduction can be achieved using various electrode materials and applied potentials, providing control over the reaction kinetics and selectivity [20].

Figure 2-2 depicts a schematic representation of a series of steps illustrating the simplified mechanism of 4-AP synthesis through the reduction of 4-NP, which has been proposed in previous publication works [2, 20, 29]. The hydrogenation of nitroaromatics faces competition from electro-hydrodimerization and HER, necessitating a balance between organic species and hydrogen intermediates for optimal electrocatalytic reduction performance [8]. However, these dimers or azo compounds might be able to change into 4-AP under certain conditions or with extra steps in the reaction. However, the efficiency and feasibility of converting these byproducts to the desired 4-AP can vary depending on the specific chemical nature of the intermediates and the reaction conditions [8, 20].

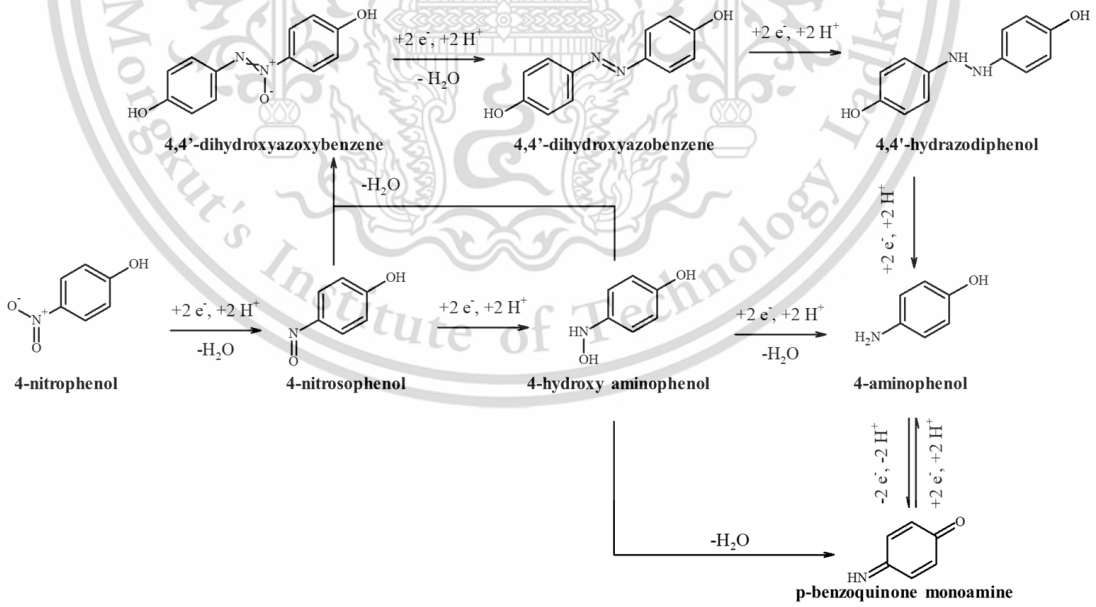

Figure 2-2 Mechanism of 4-AP synthesis through reduction of 4-NP

2.2.2 Application of 4-aminophenol

4-AP holds multifaceted importance across several industries and research domains owing to its diverse chemical properties. In the pharmaceutical sector, it serves as a vital precursor in the synthesis of numerous pharmaceutical compounds, playing a pivotal role in the production of drugs like paracetamol (acetaminophen), a widely utilized analgesic and antipyretic medication. Furthermore, 4-AP is an integral component in hair dye formulations, contributing as a color precursor in oxidative hair dyes and hair coloring products, thereby influencing the cosmetic industry. Its significance extends to the field of photography, where it functions as a developer, aiding in the reduction of silver halides to metallic silver, crucial in photographic film and print development. Additionally, 4-AP finds applications in polymer and resin production, serving as a monomer or intermediate and contributing to various polymeric materials such as coatings, adhesives, and plastics. Moreover, in laboratory settings, 4-AP is utilized as an analytical reagent for colorimetric assays and spectrophotometric analysis, enhancing its value in research and analytical domains. Its versatility across these sectors underscores its importance as a versatile compound with widespread industrial and research applications [13, 30].

2.3 Experiment designs for electrochemical toward HER and *e*-NPR

2.3.1 Competitive of HER and e-NPR

The competitiveness between the hydrogen produced and the reduced products, such as 4-AP derived from 4-NP, in an electrochemical reduction process is determined by the selectivity and efficacy of the product formation. Preferring the production of the desirable reduced product over hydrogen evolution is a competitive necessity. This is accomplished by optimizing the properties and reaction conditions of the electrocatalyst in order to increase its selectivity and efficacy with respect to the desired product. The primary objective of a competitive process is to direct the electrochemical current in a manner that maximizes the generation of the desired reduced product, while minimizing the simultaneous production of hydrogen. This optimization technique guarantees increased process efficiency and potential for practical implementation in diverse domains, including chemical synthesis and environmental remediation, where the production of particular reduced products is crucial for targeted applications. In the realm of electrochemical reduction, competitiveness is achieved by optimizing selectivity and efficiency with respect to the intended product, while simultaneously

minimizing the emission of hydrogen as a competing pathway. The competition arises in the quest for versatile catalysts and materials that can effectively support both HER and *e*-NPR, enabling dual-purpose electrochemical systems that align with sustainable and green chemistry principles, offering potential cost savings and improved resource utilization [20, 28, 31].

2.3.2 Electrodes designs toward HER and e-NPR

Electrode designs aimed at enhancing the Hydrogen Evolution Reaction (HER) have become a focal point in advancing renewable energy technologies. In the quest for clean and efficient hydrogen production, researchers are focusing on the development of novel electrode materials and structures. Traditional HER catalysts have often relied on expensive and scarce platinum-based materials, but the search for more cost-effective and sustainable alternatives has led to the exploration of various metal compounds and composites. These new designs aim to optimize the catalytic activity of electrodes, enabling them to reduce water into hydrogen gas with improved efficiency and lower overpotentials [20, 28].

One promising approach is the use of 2D materials, such as graphene and transition metal dichalcogenides, as catalyst supports due to their high surface area and electrical conductivity. Additionally, the design of hierarchical electrode structures, incorporating nanostructures like nanowires, nanotubes, and nanoparticles, enhances the electrocatalytic performance by providing numerous active sites for the HER. The pursuit of advanced electrode designs for HER not only contributes to the development of sustainable hydrogen production but also holds the potential to revolutionize other applications, including fuel cells, water electrolysis, and energy storage systems. These innovations are vital steps toward a greener and more sustainable energy future [20, 28].

Electrode designs aimed at facilitating the electrochemical reduction of 4-NP have garnered significant attention in the fields of electrochemistry and catalysis. The electrochemical reduction of 4-NP is a crucial process in various applications, such as wastewater treatment and the synthesis of valuable chemicals. Researchers have been actively working on electrode designs that enhance the efficiency and selectivity of this reduction reaction. One prevalent approach involves the utilization of nanomaterials, such as metal nanoparticles or carbon-based nanomaterials, as electrode materials. These nanomaterials offer a high surface area and can provide abundant active sites for the electrochemical reduction of 4-NP. Additionally, the design of electrode

architectures, such as three-dimensional structures or modified electrodes with specific surface functionalization, has been explored to further improve the catalytic activity and selectivity of the reduction process. By tailoring the electrode materials and structures, researchers aim to optimize the electrochemical reduction of 4-NP, enabling its efficient conversion into 4-AP or other desired products. These electrode designs play a pivotal role in advancing the field of electrocatalysis and have practical implications for environmental remediation and chemical synthesis [26, 31].

2.3.3 Transition metal phosphide

Transition metal phosphides (TMPs) are a category of inorganic compounds that consist of phosphorus atoms bonded with transition metals. These compounds exhibit a wide range of properties that are highly advantageous for various applications. Complicated of phosphorus and transition metals such as nickel [14], iron [28, 32], or cobalt[33], these substances manifest an array of chemical and physical properties. Additionally, these phosphorus-transition metal compounds can form complex structures involving the interaction of two different transition metals, known as bi-transition metal complexes [20, 32, 34]. They are formed via the formation of strong bonds. Of particular significance are their efficacy as catalysts in hydrogen evolution and oxygen reduction reactions, both of which are indispensable processes in fuel cells and sustainable energy systems.

Their potential also encompasses the utilization of light energy in chemical transformations via photocatalysis, as well as the creation of novel electronic and magnetic materials. Transition metal phosphides, owing to their modifiable compositions and structures, remain a subject of considerable interest in the fields of materials science and chemistry, presenting substantial potential for various technological progressions [35]. **Figure 2-3** illustrates the diverse aspects of TMPs, depicting information related to their synthesis methods and applications.

The utilization of phosphorus-alloying (P-alloying) in transition metal phosphides (TMPs) offers several advantages in organic transformation reactions. Firstly, these metal phosphides remain in the metallic state even in ambient air, providing a stabilizing effect. Secondly, the introduction of phosphorus atoms into metals can modify the electronic structure, notably increasing the d-electron density around the Fermi level. This modification facilitates hydrogenation reactions, enhancing catalytic activity. Thirdly, compared to conventional heterogeneous metal catalysts with numerous active sites leading to lower catalytic efficiency, TMPs form

well-defined and singular active catalytic sites, boosting their overall performance in various reactions. The unique properties of TMPs have motivated an assessment of their catalytic activities across diverse organic transformation reactions [34, 35].

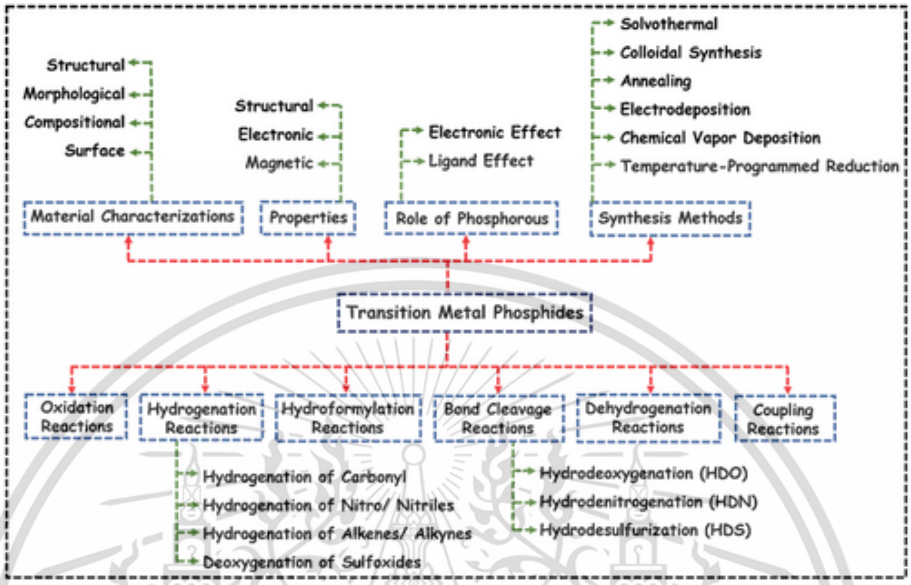

Figure 2-3 The review of various aspects of TMP [35]

Various synthesis strategies have been explored to produce TMPs, each resulting in different shapes, sizes, morphologies, and catalytic activities for specific applications. Common synthesis methods include solvothermal [36], temperature-programmed reduction (TPR) [37], annealing [38], colloidal synthesis [39], electrodeposition [14, 20], and CVD) [40]. Most of these methods involve a phosphorization step requiring high temperatures and inert atmospheres to obtain the desired TMPs. The choice of synthesis method significantly influences the morphology and subsequent catalytic activity of TMPs. Among these methods, the annealing method stands out as a simple, one-step process, making it preferable for large-scale TMPs production. Additionally, to achieve morphologically controlled TMPs, strategies such as TPR and colloidal synthesis methods are employed to tailor the desired morphology effectively [35].

2.3.4 Electrolyzer designs

An extensive exploration into the realm of electrochemical flow reactors involves a comprehensive analysis of both traditional and cutting-edge electrodes, electrocatalysts, and reactor designs. This meticulous examination delves into the fundamental principles guiding the selection of an optimal electrochemical flow

reactor, whether for small-scale laboratory experiments or large-scale pilot applications. Considerations span beyond theoretical concepts, extending to practical aspects like desired performance metrics, ease of assembly, maintenance schedules, and strategic plans for potential scalability. Integrating nanostructured electrocatalysts onto reactor surfaces stands out as a pivotal advancement, significantly enhancing reactor designs' efficiency and efficacy. Among these designs, the simplistic yet efficient parallel plate configuration, often adopted in a modular filter-press format, holds prominence across laboratory research and industrial domains [41].

The intricacies of various electrochemical cells utilized at the laboratory scale are vividly illustrated in **Figure 2-4**, which delineates the directional flow of solutions with solid arrows.

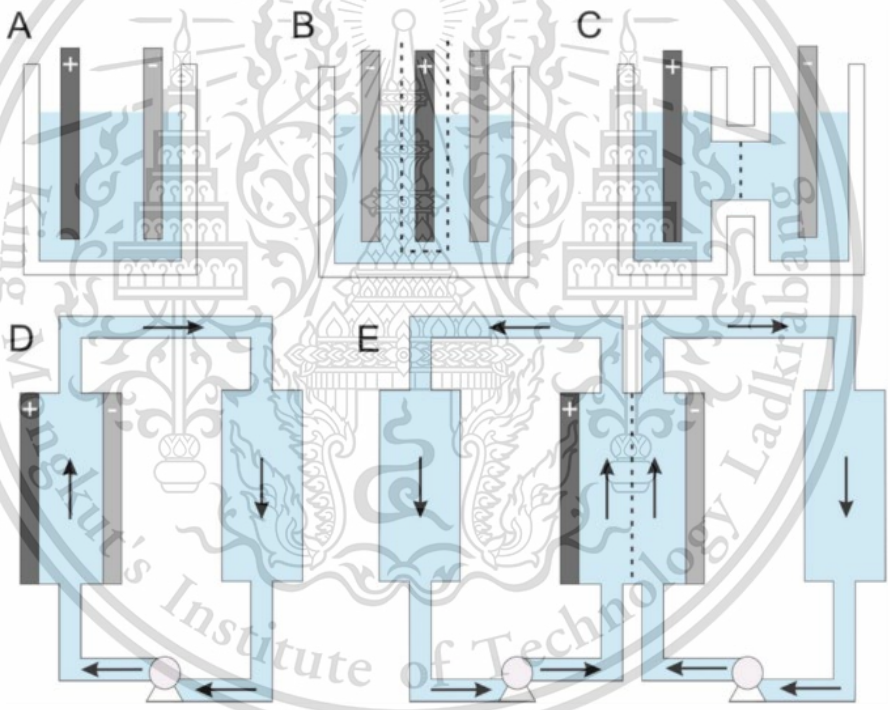

Figure 2-4 Schematics of virous electrochemical reactor: (A) Undivided beaker cell; (B) Beaker cell with the anode confined in a porous chamber; (C) Divided H-Cell with a membrane separator; (D) Undivided flow cell; and (E) Divided flow cell [41].

These configurations include the undivided H-Cell with a membrane separator, an undivided beaker cell, a beaker cell housing an anode within a porous chamber, and an undivided flow cell equipped with an electrolyte reservoir and circulating electrolyte pump. Notably, the strategic placement of anolyte and catholyte reservoirs, positioned opposite each other across a microporous membrane, plays a pivotal role in

compartmentalizing and guiding the flow within the flow cell. These depictions provide a visual narrative illustrating the diverse yet intricately designed electrochemical cells utilized in laboratory-scale experimentation, offering insights into their functionality and structural nuances [41].

This design can include porous, three-dimensional, or structured electrode surfaces and bipolar electrical connections, taking into account factors like potential and current distributions, flow uniformity, mass transport rates, electrode activity, side reactions, and current leakage within the reaction environment. Specialized electrode geometries, such as capillary gap and thin film cells, rotating cylinder electrodes, three-dimensional porous electrodes, fluidized bed electrodes, and bipolar trickle tower reactors, are also explored. Applications range from inorganic and organic electrosynthesis to environmental remediation [41, 42].

2.4 Literature reviews of electrochemical reduction of 4-NP

Electrochemistry provides significant advantages in the implementation of electrolysis processes and electrosensory technologies. Electrochemical sensors are highly effective in electrosensory applications owing to their exceptional selectivity and sensitivity. They provide instantaneous identification of target molecules in real-time and are conveniently transportable for on-site testing. Concurrently, electrochemical processes facilitate sustainable, controlled, and efficient chemical transformations during electrolysis, thereby contributing to green chemistry initiatives by minimizing environmental impact and enabling the production of valuable compounds and hydrogen. The fact that electrochemistry can be utilized for both environmentally favorable and controlled reactions, in addition to providing sensitive analytical instruments, demonstrates its immense potential in a variety of scientific, industrial, and environmental domains. In recent times, considerable attention has been devoted to the advancement and investigation of electrochemical sensors as opposed to the electrochemical reduction of 4-NP.

2.4.1 Electrochemical sensor

In order to detect 4-NP, an electrochemical sensor is generally constructed with specialized electrode materials and surface modifications that are intended to interact selectively with 4-NP molecules. By incorporating nanostructured materials into electrodes fabricated from noble metals, the sensor's sensitivity and selectivity towards 4-NP are significantly improved. The process of functionalizing the electrode surface

using molecularly imprinted polymers or specific receptors enables the identification of 4-NP. This identification results in discernible alterations in electrical characteristics or the production of unique signals, which are subsequently transduced and converted into quantifiable electrical responses. By employing methodologies such as cyclic voltammetry or impedance spectroscopy, these sensors provide expeditious and precise identification of 4-NP concentrations, thereby accommodating a wide array of uses in fields including biomedical analyses, industrial quality control, and environmental monitoring [16, 28, 43].

The electrochemical reduction of 4-nitrophenol (e-NPR) is intricately dependent on the pH environment and the specific characteristics of various catalysts. Iron-based catalysts, such as microNiFeP [20], $NiFe_2O_4$-rGO/GCE [16], single sheet iron oxides [44], and ZnO/Fe0/Fe_3C/graphitic carbon, exhibit a pH-dependent behavior. These catalysts initially demonstrate heightened reduction currents up to a pH of 7.0, after which a decline occurs at higher pH values. This phenomenon is attributed to electrostatic interactions: as the pH increases, the electrode surface becomes increasingly negatively charged, repelling the negatively charged 4-nitrophenol (4-NP) molecules and reducing their availability at the electrode surface. Modified Fe electrodes like CeFeP [28] exhibit optimal activity at a slightly acidic pH of around 5 but may encounter reduced stability in alkaline conditions at elevated temperatures [31].

In contrast, nickel-based catalysts, including Ag/Ni–MOF [45], CeO_2/Ni-MOF [46], Ni-MOF/NF [47], and NiB_x/nickel foam [7], display higher effectiveness in strongly alkaline conditions. This aligns with the behavior of nickel-based catalysts in the hydrogen evolution reaction (HER), where they exhibit heightened activity in strongly acidic or basic electrolytes. As the pH increases, the lower concentration of H^+ ions reduce the formation of adsorbed H atoms, resulting in lower activity. However, in strongly basic electrolytes, the formation of Ni oxides and hydroxides under an applied potential enhances their activities. To boost activity under near-neutral pH conditions, nickel catalysts may be augmented by co-catalysts such as Ni_3Se_4/rGO, particularly at a pH of 5.

Titanium catalysts, especially those exposing [001] facets and featuring oxygen vacancies like TiO_2 [9], exhibit enhanced activity in weakly acidic conditions, approximately at a pH of 5. In these conditions, electrons are more likely to couple with H+ ions, accelerating the reduction of p-NP via the Volmer mechanism. However, in

alkaline pH environments (pH 8.0–9.0), where p-NP molecules carry a negative charge, strong electrostatic repulsion between the negatively charged p-NP and the cathode inhibits efficient reduction compared to acidic conditions.

Bismuth catalysts like BiFEs and BNCE [43] display notable e-NPR activity around pH 5, showcasing the sensitivity of their catalytic activities to the surrounding pH environment. These insights underscore the pH-sensitive nature of various catalysts, illuminating their distinct behaviors and optimal pH conditions for facilitating the electrochemical reduction of 4-nitrophenol.

2.4.2 Electrochemical reduction/hydrogenation of 4-NP

The electrochemical reduction or hydrogenation of 4-NP signifies a significant transformation in which 4-NP is utilized to produce 4-AP, which is 4-NP's amine derivative. The reduction takes place at the surface of the electrode, assisted by particular electrocatalysts and under customized reaction conditions. During this procedure, electrons are transferred from the electrode to 4-NP, which results in the elimination of its nitro group ($-NO_2$) and the subsequent creation of an amino group ($-NH_2$). This process ultimately yields 4-AP. The pathway for this reduction may traverse a multitude of routes, each involving intermediary species and being impacted by variables such as the electrocatalyst utilized, pH levels, applied potential, and numerous other conditions. Electrochemical reduction offers several benefits, including the ability to precisely regulate reaction parameters, potential for optimizing catalysts, and encouraging applications in the development of sustainable synthesis routes. The enhancement of catalyst performance and reaction parameters is critical for increasing the yield, selectivity, and efficiency of the intended product, while simultaneously reducing undesired byproducts or side reactions. This highlights the possibility of developing synthetic pathways that are environmentally sustainable.

An eco-friendly substitute for traditional chemical-driven reactions that depend on sacrificial reagents, the dual electrochemical system developed by P. L. Zhang et al. [7] was designed to oxygenate and hydrogenate organic compounds. They fabricated NiBx@NF as the working electrode (WE) and water as the hydrogen source, using the hydrogenation of 4-NP as a model reaction. Additional research was conducted using chronoamperometry to determine the catalytic efficiency of NiBx@NF in the 4-NP hydrogenation process. Succeeding by 50 minutes at an applied potential of -0.83 V versus SHE, the catalyst produced results of ≥99% conversion and selectivity.

S. T. Wu et al. [8] proposed $CuCo_2O_4$ spinel supported on nickel foam (NF) was synthesized using a hydrothermal process and calcination, enhancing its electrocatalytic performance. The $CuCo_2O_4$/NF cathode showed exceptional results in p-nitrophenol hydrogenation, with a conversion rate and selectivity of 95.8% and 97.2%, respectively. Its Faraday efficiency remained high at 89.0% even at 240 mA cm^{-2}, indicating potential for industrial applications. The cathode also showed favorable yields in hydrogenating substituted nitroaromatics.

C. C. Ni et al. [9] investigates the synergistic role of electron-trapped oxygen vacancy and [001] facets in TiO_2 electrochemical activity towards 4-NP reduction. The combination of these facets improved the efficiency of TiO2 electrochemical reduction. Density functional theory calculations showed that the introduction of these facets and electron-trapped oxygen vacancy on TiO_2 facilitates electron transfer and improves indirect reduction efficiency. The maximum electron-trapped oxygen vacancy amount was achieved at 350°C, resulting in a 99.3% p-NP reduction efficiency.

S. C. Huang et al. [20] investigates the electrochemical synthesis of micro-structured nickel-iron phosphide (*micro*NiFeP), which is an efficient electrocatalyst for hydrogen evolution reaction (HER) and *e*-NPR at neutral pH. The *micro*NiFeP, prepared with optimized conditions, consists of submicron-sized spheres with wrinkled surfaces and exhibited promising HER activity. In the presence of 4-NP, it showed high *e*-NPR activity and selectivity against HER. It also enabled conversion of 89.6 ± 3.3 % for 4-aminophenol production after 8-hour-controlled-potential electrolysis. Mechanistic studies reveal that *e*-NPR at *micro*NiFeP involves electron transfer and the formation of 4,4'-dihydroxyazobenzene as a side product.

X. L. Pang et al. [48] presented a highly efficient catalyst known as Cu foam adorned with $Cu(OH)_2$ (CF-$Cu(OH)_2$), which they utilized to oxidize HMF. The authors utilized CuOOH active species, which were produced via electrochemistry, as the principal catalytic sites. Furthermore, the improved electrocatalyst demonstrated exceptional efficiency in the reduction of 4-NP. As the bias potential increased, so did the rate of the reaction; it peaked at a greater negative potential. It is worth mentioning that the electrocatalytic reduction of 4-NP was carried out without the requirement of argon gas protection or shielding. This resulted in an impressive 96.8% faradic efficiency and a conversion rate of nearly 100%.

CHAPTER 3
RESEARCH METHODOLOGY

3.1 Materials and equipment

Table 3-1 List of chemicals and materials

Name	Brand	Specification
Nickel(II) chloride hexahydrate	Alfa Aesar	99.3%
Sodium hypophosphite monohydrate	Alfa Aesar	≥ 99%
Ferrous(II) sulfate heptahydrate	Sigma-Aldrich	≥ 99%
Ammonium chloride	Sigma-Aldrich	99.5%
Sodium phosphate monobasic anhydrous	Sigma-Aldrich	≥ 98%
Sodium phosphate dibasic anhydrous	Sigma-Aldrich	≥ 98%
Sodium sulfate	Sigma-Aldrich	99%
Sulfuric acid	Sigma-Aldrich	1 M, 2N
Sulfuric acid	J.T. Baker	97%
Hydrochloric acid	Sigma-Aldrich	37 %wt
Nitric acid	Sigma-Aldrich	65%
Methanol	Echo Chemical	95%
Ethanol	Echo Chemical	95%
Acetone	Echo Chemical	99%
Potassium chloride	Sigma-Aldrich	≥ 99%
Sodium hydroxide	Sigma-Aldrich	≥ 98%
4-nitrophenol	Alfa Aesar	99%
4-aminophenol	Alfa Aesar	98%
Nitrogen	雲山氣體	Purity ≥ 99.99%
Nitrogen + Methane	雲山氣體	98% N_2 and 2% CH_4
Carbon paper	Alfa Aesar	TPG-H-60
Platinum foil	佳佑企業	Exposed area ~ 4 cm^2
Proton-exchange membrane (Nafion 117)	Alfa Aesar	Thickness 0.18 mm
Copper tape	3M	Type-1181

Table 3-1 List of chemicals and materials (cont.)

Name	Brand	Specification
Teflon tape (PTFE)	-	
Paraffin film	Bemis	PM992
DIW	-	Resistivity of 18.2 MΩ cm

Table 3-2 List of equipment and measurement

Name	Brand	Series
Potentiostat/Galvanostat	Ch Instrument	760E
Potentiostat/Galvanostat	Ivium Technologies	Iviumn-Stat
Ultrasonic cleaning	DELTA	DC200
Gas chromatography	Agilent	7820A
UV-Vis spectroscopy	Agilent	Cary 60
High performance liquid chromatography	Shimadzu	LC-2040C 3D
pH meter	SUNTEX	SP-2100
Inductive coupling plasma optical emission spectrometer (ICP-OES)	Horiba Jobin Yvon	JY 2000-2
X-ray diffraction (XRD)	Bruker	D8 DISCOVER
X-ray photoelectron spectroscopy (XPS)	ULVAC-PHI	PHI 5000 VersaProbe
Scanning electron microscopy (SEM)	Hitachi	SU-8010
Raman spectroscopy	RAMaker	BEII
Ultra-high performance liquid chromatography–tandem with mass spectrometry (UHPLC-MA)	Thermo Scientific™	Dionex Ultimate™ 3000 UHPLC system and a Q Exactive™ Plus Hybrid Quadrupole-Orbitrap™ Mass Spectrometer

3.2 Electrosynthesis of electrocatalysts

3.2.1 Synthesis of nickel-iron-phosphorus on carbon paper

The modified electrocatalysts of micro-structured nickel iron phosphide (*micro*NiFeP) were synthesized by electrochemical deposition at a constant cathodic current density (I_{dep}) of -20 mA cm^{-2} until the total charge passage reached 0.54 C cm^{-2}, which was connected to a three-electrode system in a single-compartment electrochemical cell utilizing a CHI 760E potentiostat as shown in **Figure 3-1**. Carbon paper as the working electrode, Pt foil (exposed area 4.0 cm^2) as the counter electrode, and Ag/AgCl (sat'd KCl) as the reference electrode. The deposition electrolyte solution contained 0.25 M of ammonium chloride, 1 M of hypophosphite, nickel chloride, and ferrous sulfate. The electrodeposition conditions as the nickel to iron molar ratio (r_{NiFe}) was adjusted to modify the composition and electrocatalytic properties of the *micro*NiFeP|CP electrodes. The r_{NiFe} was optimized (0 (*micro*FeP|CP), 0.5, 2, and infinite (inf.; *micro*NiP|CP)) with a fixed total metal of 0.2 M. Note that every deposition process was purged with N_2 to prevent the oxidation of metal by dissolved oxygen. Carbon papers were cleaned with ultrasonics in nitric acid (5 min), ethanol (5 min), and DIW (10 min), respectively [15, 20].

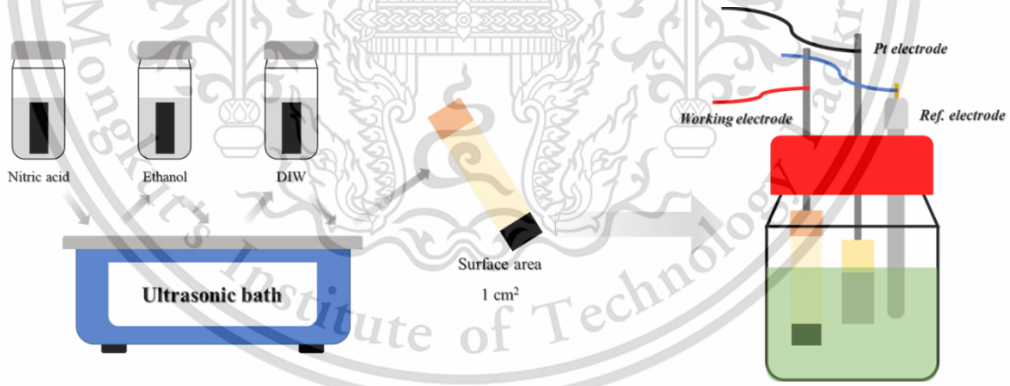

Figure 3-1 Equipment setup of fabrication of *micro*NiFeP|CP electrodes

3.2.2 Synthesis of oxide/hydroxide species on electrocatalysts

The oxide/hydroxide species of electrocatalysts were prepared by CV-pretreatment, which was connected to a three-electrode system in a single-compartment electrochemical cell utilizing a CHI 760E potentiostat, including CV-pretreated *micro*NiP|CP and CV-pretreated *micro*FeP|CP electrodes. The CV-pretreated *micro*NiP|CP electrode was prepared by subjecting the *micro*NiP|CP electrode to the

potential cycling in 0.1 M NaOH at a scan rate of 50 mV s^{-1} between 0.8 and 1.8 V vs. RHE for 225 cycles. The CV-pretreated *micro*FeP|CP electrode, on the other hand, was prepared by subjecting the *micro*FeP|CP electrode to the potential cycling in 0.1 M NaOH at a scan rate of 50 mV s^{-1} between -0.25 and 1 V vs. RHE for 225 cycles. Note that all electrolytes were purged with N_2 to reduce dissolved oxygen.

3.3 Physical characterization

The surface morphology and chemical composition of the prepared electrodes were analyzed using scanning electron microscopy (SEM) energy-dispersive X-ray spectroscopy (EDX) with a Hitachi SU-8010 microscope. An inductive coupling plasma optical emission spectrometer (ICP-OES, Horiba Jobin Yvon JY 2000-2) was utilized to measure the quantity of nickel, iron, and phosphate species on modified electrode surfaces. X-ray photoelectron spectroscopy (XPS) with a PHI 5000 VersaProbe system (ULVAC-PHI, Chigasaki, Japan) was used to investigate the elemental composition and oxidation state of the metal species on the surface of the prepared electrode and the C 1s peak at 284.8 eV of obtained XPS spectra was the binding energy scale referenced. The crystal structure of modified electrode was analyzed by using X-ray Diffraction (XRD). Raman spectra of the prepared electrodes were analyzed with a RAMaker Raman spectrometer (BEII) equipped with a 532 nm laser.

3.4 Electrochemical analyses

The all-electrochemical characterizations of *micro*NiFeP|CP electrodes were carried out with the Iviumn-Stat workstation using a three-electrode device including *micro*NiFeP|CP working electrode, platinum foil (exposed area 4.0 cm^2) counter electrode, and Ag/AgCl (sat'd KCl) reference electrode at ambient temperature. The electrochemical activity of *micro*NiFeP|CP electrodes was operated in a batch simulation with a well-sealed customized two-chambers (H-cell) cell separated with Nafion® 117 film as shown in **Figure 3-2**. The electrochemical analyses used the phosphate buffer (PBS; 0.5 M, pH 7) with and without 4-NP (4 mM) as electrolytes under N_2 purge and stirred at 900 rpm. All the reported potentials were 95% iR-compensated and referred to the reversible hydrogen electrode (RHE) using **Eq. 3-1**:

$$E(V\ vs.\ RHE) = E(V\ vs.\ Ag/AgCl) + 0.197 + 0.059 \times pH - 0.95 \times iR \quad \textbf{(3-1)}$$

Note that all fresh *micro*NiFeP|CP electrodes were pretreated by applied cyclic voltammetry (CV), in which 10 cycles of scanning ranged from 0.02 to -0.2 V vs. RHE at a scanning rate of 10 mV s^{-1} with PBS (0.5 M, pH 7). The optimized parameters toward e-NPR were operated with the batch system electrolyzer (H-cell), while the scalable system was carried out with a circulation flow-system electrolyzer. Note that all electrolysis tests were purged with N_2 to prevent the oxidation by dissolved oxygen.

3.4.1 Electrochemical properties of microNiFeP|CP

The linear sweep voltammetry (LSV) was used to measure the electrochemical properties of *micro*NiFeP|CP electrodes for the electrochemical hydrogen evolution reaction (HER) and the electrochemical reduction of 4-NP (*e*-NPR) at a scanning rate of 10 mV s^{-1} from the open circuit potential (OCP) to -0.5 V vs. RHE. The cyclic voltammetry (CV) was performed in 3 cycles with a potential window of 1 to -0.5 V vs. RHE at various scanning rates of 10, 50, 100, 200, and 250 mV s^{-1} to briefly investigate e-NPR's phenomena on *micro*NiFeP|CP. All electrochemical property studies were carried out in 0.5 M PBS without and with 4 mM 4-NP and stirred at 900 rpm. Note that all electrolysis tests were purged with N_2 to prevent the oxidation by dissolved oxygen.

3.4.2 Batch-system electrolyzer (H-cell) toward e-NPR

Electrocatalytic activity and kinetic reactions of *micro*NiFeP|CP electrodes toward *e*-NPR were investigated by controlled-potential electrolysis (CPEs) in 0.5 M PBS containing 4 mM of 4-NP with stirred at 900 rpm, as shown in **Figure 3-2**. 4-h CPEs at -0.15 V vs. RHE were carried out to investigate and optimize the composition of electrodeposited electrolytes, as nickel iron ratio (r_{NiFe}). After that, 1-h CPEs at 0.10, 0.05, 0.00, -0.05, -0.10, and -0.15 V vs. RHE were performed in various pH values (5.0, 7.0, and 9.0) to investigate the activity and performance toward *e*-NPR with the optimized *micro*NiFeP|CP electrodes which prepared with $C_{hypophosphite}$ = 1 M and r_{NiFe} = 0.5. Finally, potential and reaction time were considered key parameters toward *e*-NPR. Note that the electrolysis products were evaluated using HPLC and UV-Vis, as discussed in **Section 3.5**, and all electrolysis tests were purged with N_2 to prevent the oxidation by dissolved oxygen.

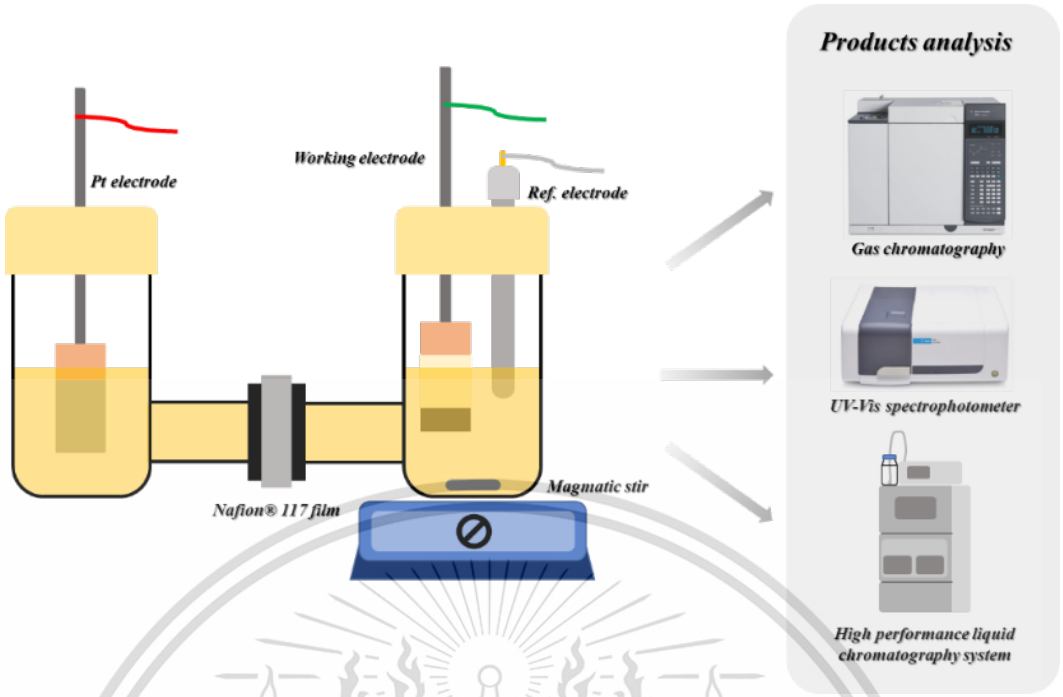

Figure 3-2 Equipment setup of electrochemical analysis with H-cell electrolyzer.

3.4.3 Circulation flow-systems electrolyzer toward e-NPR

To improve the performance of *e*-NPR, *micro*NiFeP|CP electrodes were investigated by controlled-current electrolysis (CCEs) with a flow-system electrolyzer separated with Nafion® 117 film in circulation operation mode at a flow rate of 200 mL min^{-1} as shown in **Figure 3-3**. 1-h CCEs at -10, -20, -50, and -100 mA cm^{-2} were investigated the activity and performance toward e-NPR with the optimized *micro*NiFeP|CP electrodes in 0.5 M PBS containing 4 mM of 4-NP. After that, 3-h CCEs at -10 mA cm^{-2} were carried out in 0.5 M PBS containing 10 mM of 4-NP to scale up, which *micro*NiFeP|CP*op* as working electrode with geometry area 6.25 cm^{-2} and Ag/AgCl reference electrode were placed in the cathodic compartment, whereas Pt counter electrode was placed in the anodic compartment. For comparison, the 3-h CCEs at -10 mA cm^{-2} was performed with batch-system electrolyzer (H-cell) as the same conditions with flow-system electrolyzer. Note that the electrolysis products were evaluated using HPLC and UV-Vis, as discussed in **Section 3.5**, and all electrolysis tests were purged with N_2 to prevent the oxidation by dissolved oxygen.

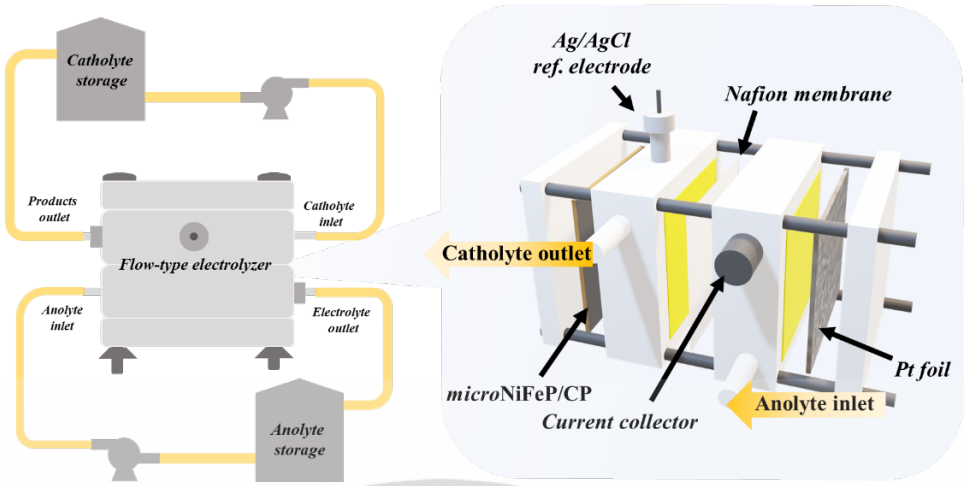

Figure 3-3 Equipment setup of electrochemical analysis with flow-system electrolyzer.

3.5 Products analysis

The determination of 4-NP concentration was measured by UV-Vis spectrophotometer with scanning window between 250 and 500 nm. 4-NP solutions were diluted 30 time in 0.5 M PBS and adjust pH reached 12 with sodium hydroxide to deprotonation of 4-NP, which were detected at λ = 400 nm. The measured absorbance at λ= 400 nm of deprotonation of 4NP was converted to the 4-NP concentration (C_{NP}) using a pre-determined calibration curve [2, 22]. Concentration of 4-NP before ($C_{NP,0}$) and after (C_{NP}) e-NPR were calculated the conversion (%) of 4-NP using **Eq. 3-2**:

$$Conversion(\%) = \frac{C_{NP,0} - C_{NP}}{C_{NP,0}} \times 100\% \quad \textbf{(3-2)}$$

The generated gaseous products (i.e., H_2 gas) from *e*-NPR were analyzed and quantified using an Agilent 7890A Series gas chromatography (GC) equipped with a thermal conductivity detector (TCD) and 5 Å molecular sieve column that was holding temperature at 40 °C. The liquid products (i.e., 4-AP) were quantified by a Shimadzu Nexera-I LC-2040C 3D high performance liquid chromatography system (HPLC) equipped with a Shodex HILICpak VG-50 4E column (250 × 4.6 mm, 5 µm, 100 Å), combined with Shodex HILICpak VG-50G 4A column guard (10 × 4.6 mm, 5 µm, 100 Å), and a photodiode array detector (λ = 233 nm). The analysis was performed in isocratic mode with mobile phase of DIW and methanol (volume ratio: 1:1) at flow rate of 0.6 mL min^{-1}, temperature of column at 40 °C, which was injected 10.0 µL to analyze. The Faradaic efficiency for H_2 (FE_{H2}; **Eq. 3-4**) was determined by the

generated amount of H_2 (N_{H2}), whereas the Faradaic efficiency (FE_{AP}; **Eq. 3-3**), selectivity (S_{AP}; **Eq. 3-6**), and electron transfer number (n_{eNPR}; **Eq. 3-5**) for generated 4-AP were determined by the amount of 4-AP (N_{AP}) for each CPEs and CCEs.

$$FE_{AP}(\%) = \frac{6F \times N_{AP}}{Q_{total}} \times 100\% \quad \textbf{(3-3)}$$

$$FE_{H2}(\%) = \frac{2F \times N_{H2}}{Q_{total}} \times 100\% \quad \textbf{(3-4)}$$

$$n_{eNPR} = \frac{Q_{Total} \times (1\text{-}FE_{H2})}{\Delta N_{NP} \times F} \quad \textbf{(3-5)}$$

$$S_{AP}(\%) = \frac{N_{AP}}{V_{catholye} \times (C_{NP,0} - C_{NP})} \times 100\% \quad \textbf{(3-6)}$$

where Q_{total} is the total charge passage, $V_{catholyte}$ is the volume of the catholyte, and F is the Faradaic constant (96485 C mol^{-1}). The total current density (J_{total}), partial current density of hydrogen gas (J_{H2}), and partial current density of produce 4-AP from e-NPR (J_{AP}) were derived from **Eq. 3-7**, **Eq. 3-8**, and **Eq. 3-9** , respectively [20]:

$$J_{total} = \frac{Q_{total}}{t_{CPE}} \quad \textbf{(3-7)}$$

$$J_{H2} = \frac{Q_{total} \times FE_{H2}}{t_{CPE}} \quad \textbf{(3-8)}$$

$$J_{total} = \frac{Q_{total} \times FE_{AP}}{t_{CPE}} \quad \textbf{(3-9)}$$

Turnover frequency for the evaluation of the electrocatalytic activities towards the generation of 4-AP from *e*-NPR (TOF_{AP}) at the duration of CPEs (t_{CPE}) was determined using **Eq. 3-10** and the ICP-OES-quantified loading amount of metal species (N_{Fe+Ni}) [15, 49]:

$$\boldsymbol{TOF_{AP} = \frac{N_{AP}}{N_{Fe+Ni} \times t_{CPE}}} \quad \textbf{(3-10)}$$

3.5.1 Analysis of products for identified side products

Products after e-NPR with the *micro*NiFeP|CP$_{OP}$ electrode was analyzed using a UHPLC-MS System consisting of a Thermo Scientific™ Dionex Ultimate™ 3000 UHPLC system and a Q Exactive™ Plus Hybrid Quadrupole-Orbitrap™ Mass Spectrometer to identify the other potential side products. The analysis was performed in isocratic mode with mobile phase of DIW and methanol (volume ratio: 1:1) at a flow rate of 0.4 mL min^{-1}, temperature of column at 40 °C, which was injected with 10.0 µL to analyze. A H-ESI (electron spray ionization) with a positive polarity ([M+H]$^{+}$) mode was used as an ion source, and the analysis was performed in the full mass range, which tracks products ranging from m/z of 90 Da to 1000 Da. The ionization parameters were adjusted as follows: The spray voltage utilized in the experiment was 1.5 kV, while the sheath gas pressure and auxiliary gas pressure were maintained at 35 psi and 10 psi, respectively. To prepare samples, the catholyte solution after 3-h constant-current electrolysis (CCEs) using the flow-type electrolyzer was diluted 20 times with DIW.

CHAPTER 4
RESULT AND DISCUSSION

In prior research, the physical properties of electrochemical deposition and electrochemical catalytic activity toward HER of the modified electrocatalysts of submicron-structured nickel-iron phosphide electrodes (*micro*NiFeP) prepared with facile and scalable electrochemical deposition were described. In addition, the *micro*NiFeP electrode with optimal HER activity was briefly applied toward electrochemical hydrogenation of 4-NP at neutral pH [15, 20]. To further investigate and comprehend *e*-NPR with micron-structured nickel iron phosphide electrodes on carbon paper (*micro*NiFeP|CP), the optimization of the nominal Ni^{2+}/Fe^{2+} molar ratio (r_{NiFe}) on the electrochemical deposition of *micro*NiFeP|CP electrodes toward *e*-NPR was reconsidered. In this section, sustainable and satisfactory conditions for *e*-NPR, including working potential, reaction time, and pH value with a *micro*NiFeP|CP electrode, were also considered and discussed. A flow-system electrolyzer was utilized to magnify and improve the performance of *micro*NiFeP|CP_{OP} electrodes for 4-NP remediation and uncomplicated operation. Furthermore, the mechanism pathway and active species of *micro*NiFeP|CP toward *e*-NPR were investigated and proposed.

4.1 *e*-NPR activity of *micro*NiFeP|CP electrodes various r_{NiFe} values

4.1.1 Physical characteristic of microNiFeP|CP electrodes various r_{NiFe} values

The chemical compositions of the nickel-iron phosphide film modified electrodes (*micro*NiFeP|CP) prepared in the electrolyte containing-ammonium chloride (0.25 M), hypophosphite (1 M), and various Ni^{2+}/Fe^{2+} molar ratios (r_{NiFe}; at 0 (*micro*FeP|CP), 0.5, 2, and inf.), as total metals of 0.2 M, at a cathodic current density (I_{dep}) of -20 mA cm^{-2} for 27 s (as see the **Experimental Section 3.2.1** for the details), were analyzed using ICP-OES (as shown in **Table 4-1)**. The metal species' loading amount of electrocatalytic on carbon paper was slightly different (N_{Ni+Fe}: 2.09 to 2.46 µmol cm^{-2}). For example, the *micro*NiFeP|CP (r_{NiFe} = 0.5) electrode exhibited the actual Ni/Fe molar ratio of 0.28 and N_P/N_{Fe+Ni} of 0.11. As the results in **Table 4-1**, the actual Ni/Fe molar ratios were lower than the Ni^{2+}/Fe^{2+} molar ratio (r_{NiFe}) of the plating solution. Additionally, the increasing of r_{NiFe} decreased the amount of deposited metallic and the metal/P molar ratios. In another word, the actual Ni/Fe and metal/P

molar ratio of the prepared *micro*NiFeP|CP electrodes can be controlled by adjusting the r_{NiFe} of the plating solution, which is in agreement with the previous report [16, 20, 50, 51].

Table 4-1 The physical properties of the *micro*NiFeP|CP electrodes prepared with various Ni^{2+}/Fe^{2+} molar ratio (r_{NiFe})

	r_{NiFe} used for the preparation of the *micro*NiFeP|CP electrode			
	0	**0.5**	**2**	**inf.**
N_{Ni} (µmole cm^{-2})	0.00 ± 0.00	0.47 ± 0.03	1.13 ± 0.01	2.46 ± 0.03
N_{Fe} (µmole cm^{-2})	2.33 ± 0.04	1.70 ± 0.04	0.96 ± 0.01	0.00 ± 0.00
N_P (µmole cm^{-2})	0.11 ± 0.00	0.24 ± 0.00	0.35 ± 0.00	0.56 ± 0.00
N_{Ni+Fe} (µmole cm^{-2})	2.33 ± 0.04	2.17 ± 0.04	2.09 ± 0.02	2.46 ± 0.03
N_{Ni}/N_{Fe}	0	0.28	1.17	∞
N_P/ N_{Fe+Ni}	0.05	0.11	0.17	0.23

Figure 4-1 showed the morphology of *micro*NiFeP|CP electrodes prepared with various r_{NiFe} values were analyzed using SEM, which can be found that the *micro*NiFeP|CP electrodes prepared with $r_{NiFe} \leq 0.5$ consisted of aggregates of *micron*-cubes particles with a size of ~400 nm, whereas those prepared with $r \geq 2$ contained the aggregates of the *micron*-spherical particles with a size of ~200 nm, as similar previous reported [20].

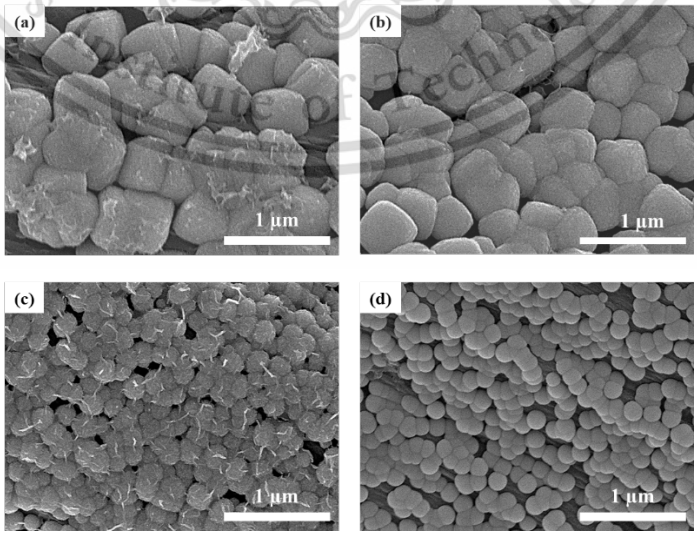

Figure 4-1 SEM of *micro*NiFeP|CP electrodes prepared with $C_{hypophosphite}$ = 1 M and various r_{NiFe} (a: 0; b: 0.5; c: 2; and d: inf.)

XRD analyses (**Figure 4-2**) showed the similarly of the phase structure of each element on *micro*NiFeP|CP electrodes. XRD results reveal that the *micro*NiFeP|CP electrodes prepared with $r_{NiFe} \leq 0.5$ displayed the diffraction peak corresponding to metallic iron (JCDS#06-0696) at 44.673˚, while $r_{NiFe} \geq 2$ displayed the weak diffraction peak corresponding to metallic nickel (JCPD#45-1027) at 44.520˚; whereas all electrodes displayed the strongest diffraction peak corresponding to carbon bare (JCPD#41-1487) at 26.381˚, 42.221˚, and 54.542˚. **Figure 4-2.**

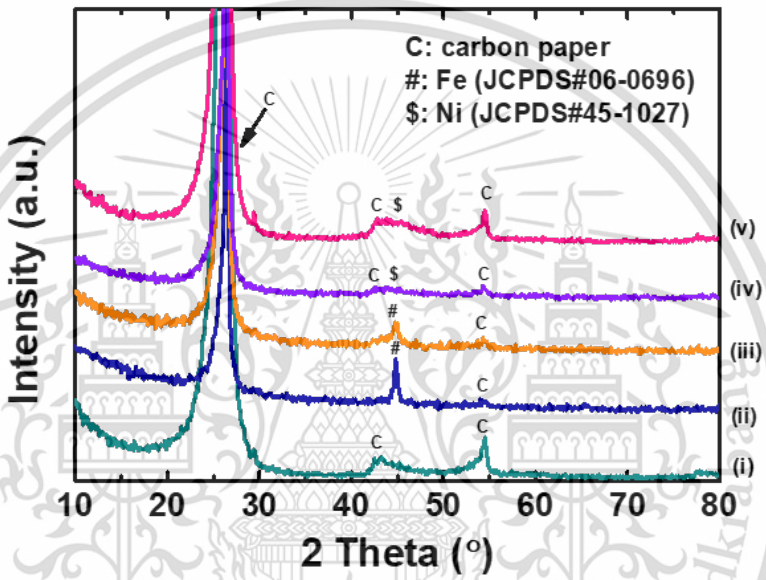

Figure 4-2 XRD of carbon paper (i) and the *micro*NiFeP|CP electrodes prepared with $C_{hypophosphite}$ = 1 M and various r_{NiFe} (ii: 0; iii: 0.5; iv: 2; and v: inf.)

Additionally, Raman features characteristics of the *micro*NiFeP|CP (r_{NiFe} = 0.5) electrode, as revealed in **Figure 4-3,** were displayed diffraction peak of the α-FeOOH (peaks at 485, 550, and 685 cm^{-1}) [52] and α-Fe_2O_3 (peaks at 221, 243, 289, 406, and 606 cm^{-1}) [53]. The presence of impurities in the *micro*NiFeP|CP (r_{NiFe} = 0.5) electrode can be attributed to two main processes; firstly, the oxidation of metallic iron occurs when it is exposed to air and secondly, the precipitation of iron hydroxides takes place due to the high local pH caused by the hydrogen evolution reaction (HER) during the electrochemical preparation of the electrode [20]. Additionally, the transformation of iron hydroxides into α-Fe_2O_3 is induced by laser irradiation during the Raman analysis, leading to the presence of impurities [53]. These findings have been reported in previous studies. The lack of discernible diffraction

peaks for α-FeOOH and α-Fe_2O_3 in **Figure 4-3** indicates that these two species may exist in an amorphous state or in relatively modest quantities.

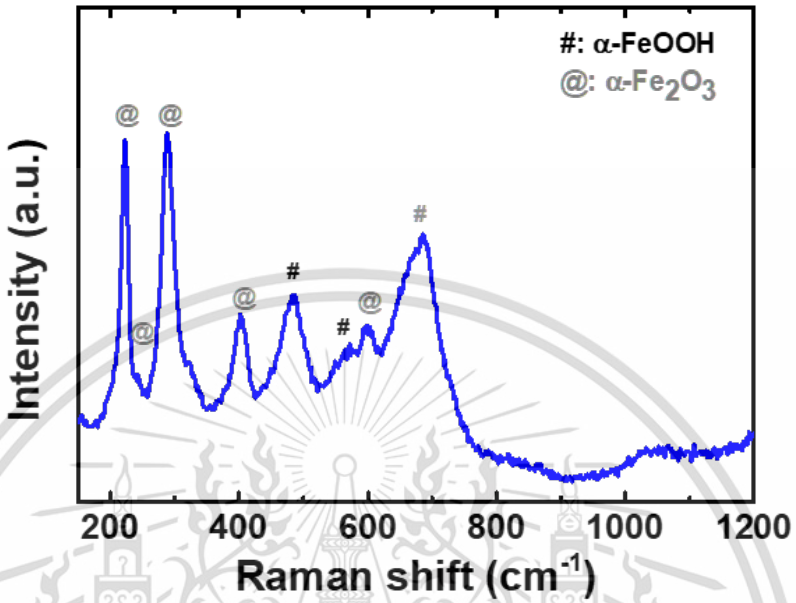

Figure 4-3 Raman spectrum of the *micro*NiFeP|CP electrodes prepared with $C_{hypophosphite}$ = 1 M and various r_{NiFe} = 0.5

Figure 4-4 shows the XPS spectra of the *micro*NiFeP|CP electrode. The presence of $Ni^{\delta+}$ species and $P^{\delta-}$ species in the Ni $2p_{3/2}$ region at 853.6 eV and the P 2p region at 130.6 eV (as shown in **Figure 4-4a** and **Figure 4-4d**, respectively) confirms the formation of nickel phosphide in the *micro*NiFeP|CP (r_{NiFe} = 0.5) electrode. Additionally, metallic nickel and metallic iron were identified in the Ni 2p3/2 region at 852.6 eV and the Fe $2p_{3/2}$ region at 706.9 eV, respectively, in the same electrode (as seen in **Figure 4-4a** and **Figure 4-4b**, respectively). Furthermore, other peaks at 856.3 eV (Ni $2p_{3/2}$), 711.3 eV and 709.7 eV (Fe $2p_{3/2}$), 532.9 eV, 531.9 eV, and 530.6 eV (O 1s), and 133.9 eV (P 2p) regions in **Figure 4-4** suggest the presence of NiOx, FeOx, and POx species in the *micro*NiFeP|CP (r_{NiFe} = 0.5) electrode. Notably, the absence of Raman features of NiOx and POx in **Figure 4-3** indicates that these species, likely formed by the oxidation of nickel phosphide upon exposure to air [54], are likely present in small amounts and primarily on the electrode's surface. Furthermore, as illustrated in **Figure 4-2** and **Figure 4-4**, the *micro*NiFeP|CP (r_{NiFe} = 0) electrode is comprised of crystalline metallic iron alongside amorphous or low-content FeOx. In

the case of the *micro*NiFeP|CP (r_{NiFe} = 2) electrode, it contained low-crystalline metallic iron, metallic nickel, nickel phosphide, NiOx, and FeOx. As for the *micro*NiFeP|CP (r_{NiFe} = inf.) electrode, it was composed of low-crystalline metallic nickel, nickel phosphide, POx, and NiOx.

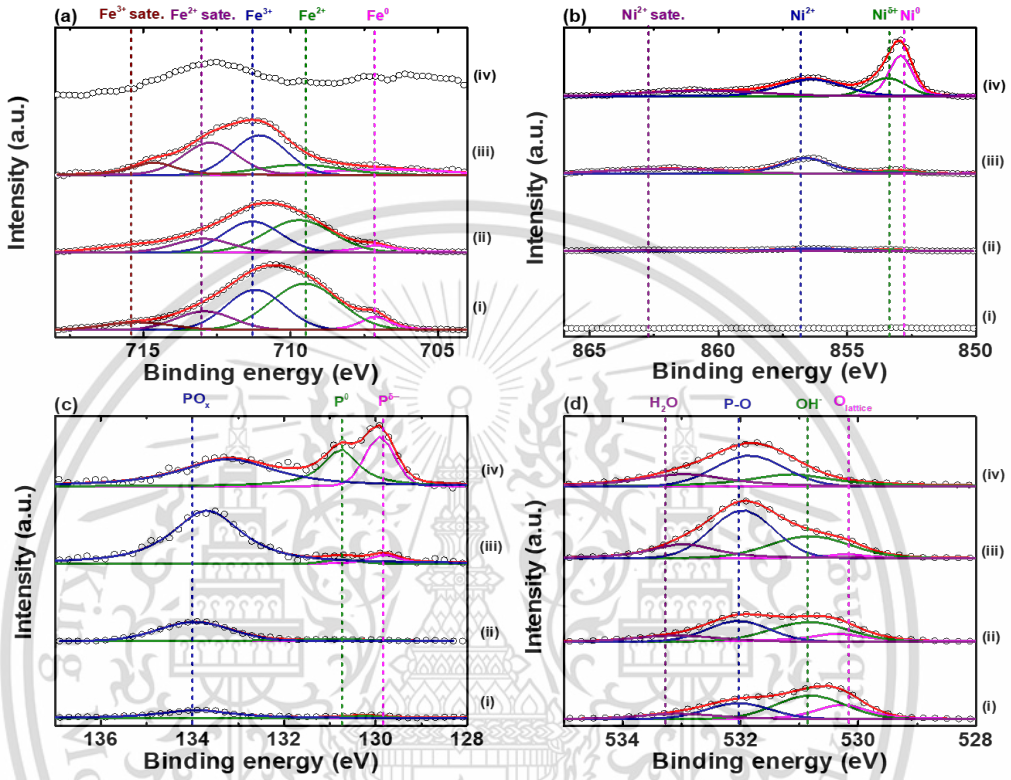

Figure 4-4 XPS of the *micro*NiFeP|CP electrodes prepared with $C_{hypophosphite}$ = 1 M and various nickel iron ratio (i: 0 (*micro*FeP|CP); ii: 0.5; iii: 2; and iv: inf. (*micro*NiP|CP)): (a) Fe 2p region; (b) Ni 2p region; (c) P 2p region; and (d) O 1s region.

4.1.2 Electrochemical activities of *micro*NiFeP|CP electrodes various r_{NiFe} values

As demonstrated by the linear sweep voltammograms (LSV) in **Figure 4-5**, *micro*NiFeP|CP electrode prepared with r_{NiFe} = inf. (*micro*NiP|CP) proposed greater electrocatalytic activity than that prepared with r_{NiFe} = 0 (*micro*FeP|CP). The electrochemical activity index is the overpotential required to obtain a geometric current density of - 10 mA cm^{-2} toward HER ($\eta_{10,HER}$) of *micro*NiFeP|CP (r_{NiFe} = 0.5) electrode (-181.5 mV) and *micro*NiFeP|CP (r_{NiFe} = 2) electrode (-215.5 mV) lower than *micro*NiP|CP electrode (-256.5 mV) and *micro*FeP|CP electrode (-428.8 mV). These results indicated that the cooperation of nickel and iron species on the *micro*NiFeP|CP

electrode improved the HER activity in comparison to electrodes prepared with *micro*NiP|CP electrode and *micro*FeP|CP electrode. In other words, the facilitated electrochemical hydrogenation activity of *micro*NiFeP|CP electrode was assumedly due to the modification of its electronic structure and the reduction of hydrogen adsorption energy caused by the incorporation of iron and nickel species [20, 32, 55]. Furthermore, the addition of 4-NP to the electrolyte caused a positive shift in the onset potential of the catalytic current and an increase in the catalytic current in the low potential region for all *micro*NiFeP|CP electrodes (**Figure 4-5**); nevertheless, the LSV results and a geometric current density of - 10 mA cm^{-2} toward *e*-NPR ($\eta_{10,NPR}$), the *micro*NiFeP|CP (r_{NiFe} = 0.5) electrode (-64.8 mV) *micro*NiFeP|CP (r_{NiFe} = 2) electrode (-118.5 mV) lower than *micro*NiP|CP electrode (-174.6 mV) and *micro*FeP|CP electrode (-418. mV), exhibited the same behavior as toward HER when r_{NiFe} values were considered, with results suggesting that *micro*NiFeP|CP electrodes favored *e*-NPR over HER [20].

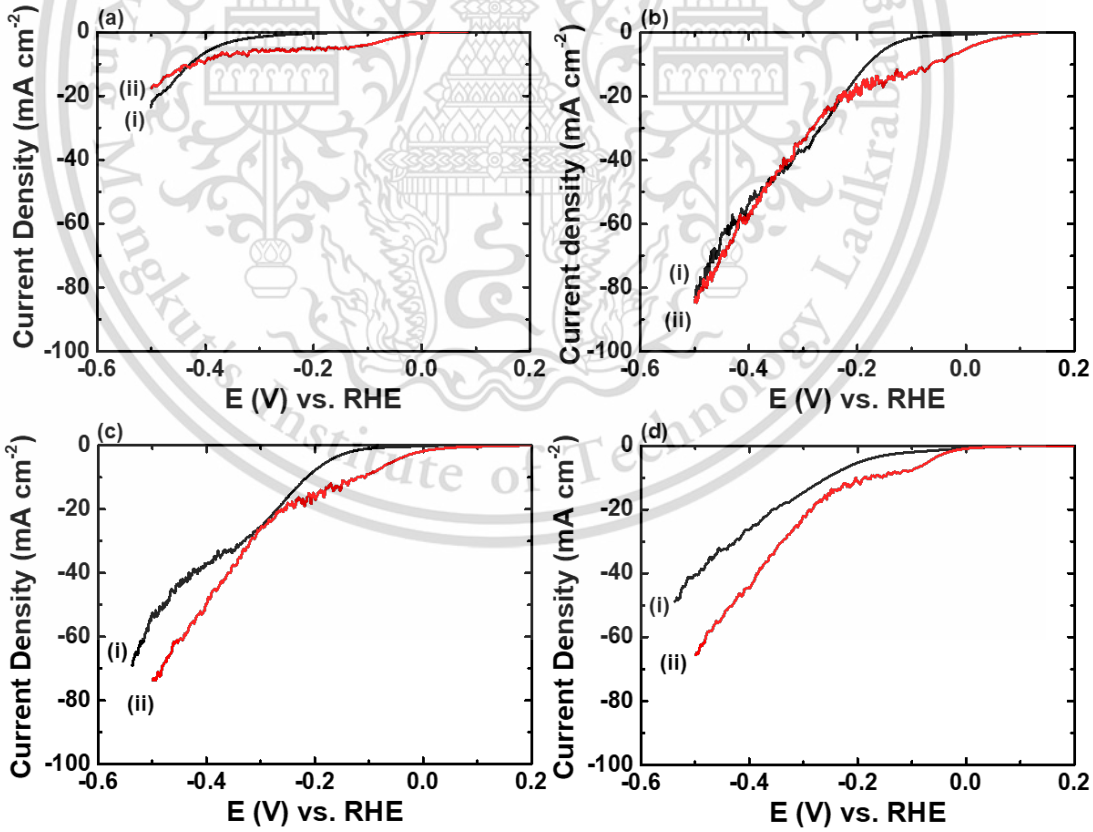

Figure 4-5 LSV of the *micro*NiFeP|CP electrodes prepared with $C_{hypophosphite}$ = 1 M and various r_{NiFe} (a: 0 (*micro*FeP|CP); b: 0.5; c: 2; and d: inf. (*micro*NiP|CP)) at 10 mV s^{-1} in phosphate buffer (0.5 M, pH 7.0) without 4-NP (black) and with 4 mM of 4-NP (red)

Moreover, the LSV results exhibited the highly competitive of HER and *e*-NPR at more negative working potential as shown in **Figure 4-5**; that indicating that the optimizing working potential of CPEs was significant parameter on *e*-NPR with *micro*NiFeP|CP (r_{NiFe} = 0.5). Therefore, the competitiveness of HER and e-NPR at nearly hydrogen evolution potential were investigated and optimized.

The electrocatalytic activities of *micro*NiFeP|CP electrodes with different r_{NiFe} values toward 4-NP (4 mM) in deaerated phosphate buffer (PBS; 0.5 M, pH 7.0) were investigated through 4-h controlled-potential electrolysis (CPEs) of 4-NP at -0.15 V vs RHE to further confirm e-NPR activity, as summarized in **Figure 4-6**. To facilitate comparisons of the electrocatalytic performance of each *micro*NiFeP|CP electrode, UV-Vis spectroscopy and HPLC were used to evaluate the electrochemical transformation of 4-NP, and GC was used to evaluate the generated hydrogen, as represented by the faradaic efficiency of 4-AP and H_2 (FE_{AP} and FE_{H2}, respectively), the conversion of 4-NP, and the selectivity of 4-AP (S_{AP}). **Figure 4-6a** shows the slightly different total charge passage of each *micro*NiFeP|CP electrodes toward *e*-NPR. Meanwhile, the obtained total current density (J_{total}; **Figure 4-6b**) exhibited similar trends to the LSV results and $\eta_{10,NPR}$ when 4-NP were contained (**Figure 4-5**). The *micro*FeP|CP electrode presented a J_{H2} of -0.0713 ± 0.0267 mA cm^{-2} which is less than the *micro*NiP|CP electrode (-0.8668 ± 0.2016 mA cm^{-2}) and *micro*NiFeP|CP (r_{NiFe} = 0.5) electrode (-0.1325 ± 0.0135 mA cm^{-2}) and *micro*NiFeP|CP (r_{NiFe} = 2) electrode (-0.6246 ± 0.1282 mA cm^{-2}), as shown in **Figure 4-6b**; else, FE_{H2} (**Figure 4-6c**) showed a nearly identical trend as J_{H2}. As a result, it can be inferred that Ni species plays an essential role in modulating the hydrogenation pathway and promoting the occurrence of preferential proton transfer with water as the hydrogen source [56]. The *micro*NiFeP|CP electrode prepared with low r_{NiFe} values showed improvement in FE_{AP} (**Figure 4-6c**) and J_{NPR} (**Figure 4-6b**); on the other hand, the excess r_{NiFe} values did not result in significance. Particularly, *micro*NiFeP|CP (r_{NiFe} = 0.5) electrode shown J_{NPR} of -4.09 ± 0.1282 mA cm^{-2} and FE_{AP} of 97.37 ± 0.79%, which is higher than *micro*NiFeP|CP (r_{NiFe} = 2) electrode (-3.26 ± 0.20 mA cm^{-2} and 82.16 ± 3.94%, respectively), *micro*NiP|CP electrode (-3.25 ± 0.18 mA cm^{-2} and 78.4 ± 4.48%, respectively), and *micro*FeP|CP electrode (-3.41 ± 0.17 mA cm^{-2} and 94.95 ± 1.39%, respectively). Moreover, the generated hydrogen bubbles produced via HER lead to reductive current efficiency and could affect the electron transfer at the electrocatalyst surface [57]. The conversion of 4-NP and selectivity of 4-AP were demonstrated in

Figure 4-6d. The *micro*NiFeP|CP (r_{NiFe} = 0.5) electrode has the highest conversion of 4-NP (70.25 ± 5.20%) as the 4-h CPEs at -0.15 V vs. RHE. While the S_{AP} of each electrocatalyst was slightly different (97.96 % to 99.24%). This finding suggests that the iron content of the activity of the *micro*NiFeP|CP electrodes towards *e*-NPR has effect on the remediation of 4-NP, but that has a negligible effect on the generated 4-AP. Moreover, it was proposed that the competitiveness of e-NPR and HER.

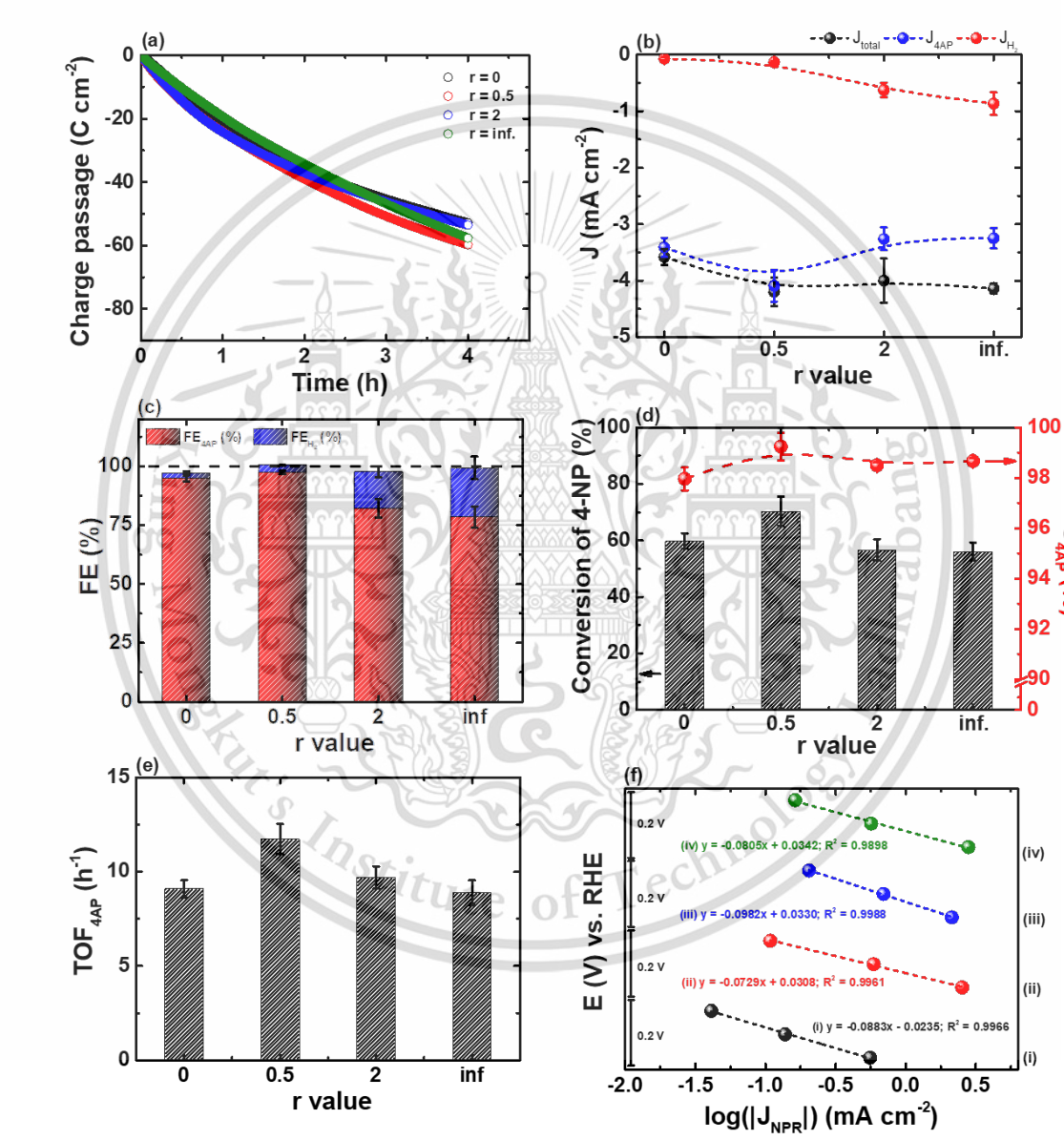

Figure 4-6 (a) Total charge passage of *e*-NPR; (b) Total current (J_{total}), current responsible of HER (J_{H2}) and e-NPR (J_{NPR}); (c) %FE of H_2 and 4-NP; (d) Conversion of 4-NP and S_{AP}; (e) TOF; and (f) Tafel plot of *micro*NiFeP|CP electrode various r_{NiFe} (i: 0; ii: 0.5; iii: 2; and iv: inf.) within 4-CPEs at -0.15 V vs. RHE in 0.5 M of PBS contained 4 mM of 4-NP.

Furthermore, the slightly increasing of r_{NiFe} values provided the highest quantifies on the turnover frequency of *e*-NPR (TOF_{AP}) in **Figure 4-6e**, which could be attributed to the conversion of 4NP and the stronger synergy of iron and nickel species toward *e*-NPR [20, 32, 55]; especially *micro*NiFeP|CP (r_{NiFe} = 0.5) electrode (11.73 ± 0.80 h^{-1}) was higher than 1.30, 1.24, and 1.43 times comparing with *micro*FeP|CP electrode (9.09 ± 0.46 h^{-1}), *micro*NiFeP|CP (r_{NiFe} = 2) electrode (9.45 ± 0.60 h^{-1}), and *micro*NiP|CP electrode (8.21 ± 0.45 h^{-1}), respectively. This finding suggests that a slight addition of nickel species to the fabrication of *micro*NiFeP|CP electrodes could enhance the benefits of iron species on the selective expression of *e*-NPR and HER, which could reduce the quantity of hydrogen produced as well as did not significantly influence on selectivity of 4-AP (S_{AP}), as shown in **Figure 4-6d**. To supporting the above discussion, the Tafel plots in **Figure 4-6f** were investigated that indicated also indicated *micro*NiFeP|CP (r_{NiFe} = 0.5) electrode was the suitable condition for electrodeposit, which showed the excellence electrochemical properties on Tafel slop (-0.072 dec^{-1}). The above discussion implied the difference in electrocatalytic activities of *micro*NiFeP|CP electrodes toward *e*-NPR and a promise for electrochemical tunability based on composition (r_{NiFe}) in deposited electrolytes [20].

4.1.3 Identification active species on electrocatalytic

To identify the active species, the *micro*NiP|CP and *micro*FeP|CP *electrodes* were pretreated with the cyclic voltammetry method (CVs) to transform into oxide/hydroxide species as shown in the **Experimental Section 3.2.2** for the details by subjecting the *micro*NiP|CP and *micro*FeP|CP electrodes to the CV-pretreatment (as shown in **Figure 4-7(a-b)**, respectively). To confirm the oxide/hydroxide species, the Raman analyses in **Figure 4-7(c-d)** range from 200 –1000 cm^{-1} indicating the surfaces of *micro*NiP|CP and *micro*FeP|CP electrodes after CV-pretreated were enriched with nickel hydroxides and iron oxides, respectively.

After subjecting the *micro*NiP|CP and *micro*FeP|CP electrodes to CV pretreatment, which were investigated the e-NPR within 4-h CPEs at -0.15 V vs. RHE. The results obtained from the 4-h CPE s (as shown in **Figure 4-8** and **Table 4-2**) reveal that the presence of an oxide or hydroxide layer has an adverse effect on the FE_{AP} and the S_{AP}. For example, the FE_{AP} and S_{AP} of the *micro*NiP|CP_{Ox} electrode were 72.80 ± 2.41% and 89.75 ± 2.41%, respectively. The pristine *micro*NiP|CP electrode had higher values, with FE_{AP} at 78.4 ± 4.48% and S_{AP} at 98.66 ± 0.12%. However, the FE_{AP} and S_{AP} of the *micro*FeP|CP_{Ox} electrode were 89.78 ± 0.36% and 92.72 ± 0.47%,

respectively. The unmodified *micro*FeP|CP electrode had better results, with FE_{AP} of 94.95 ± 1.39% and S_{AP} of 97.79 ± 0.46%.

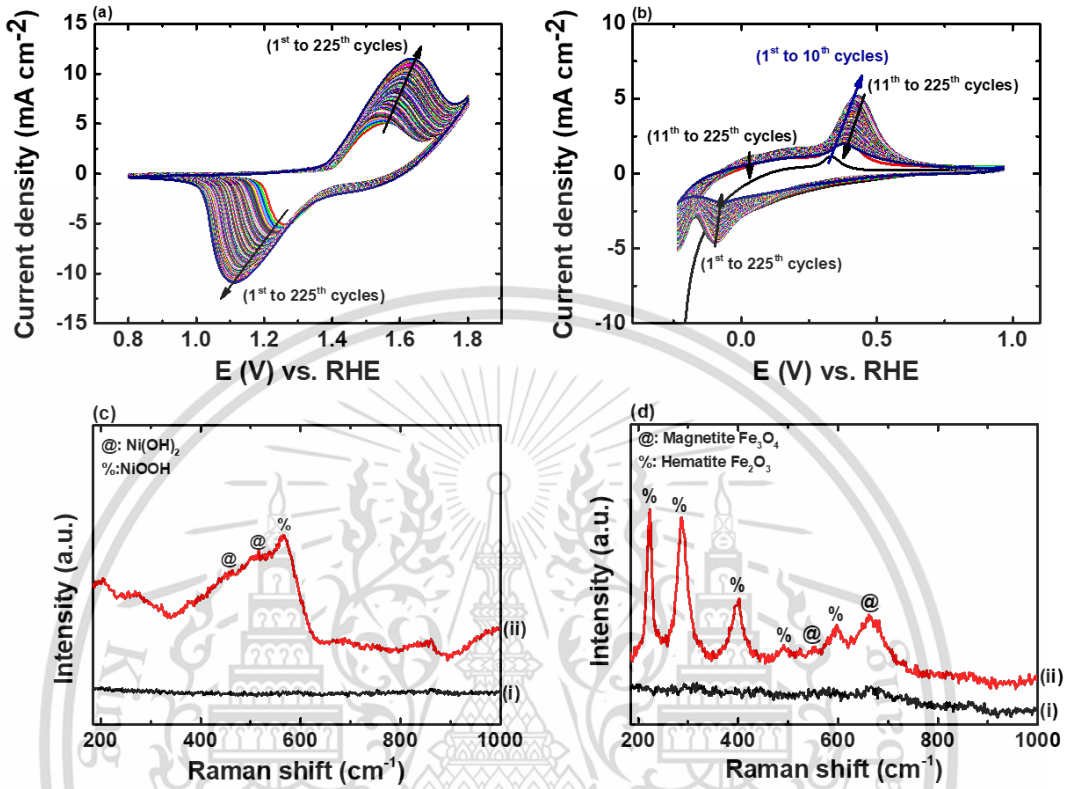

Figure 4-7 (a-b) CVs recorded during the CV-pretreatment of at a scan rate of 10 mV s^{-1} in 0.1 M NaOH solution and (c-d) Raman spectra: (a,c) the *micro*NiP|CP electrode and (b, d) the *micro*FeP|CP electrode: (i) pristine and (ii) after CV-pretreated.

Table 4-2 Results of 4-h CPE at -0.15 V vs. RHE using the *micro*NiP|CP_{Ox} and *micro*FeP|CP_{Ox} electrodes in phosphate solution (0.5 M, pH 7) containing 4-NP (4 mM)

	Electrodes	
	*micro*NiP|CP_{Ox}	*micro*FeP|CP_{Ox}
Charge passage (C cm^{-2})	-81.16 ± 3.23	-45.12 ± 5.23
FE_{AP} (%)	72.80 ± 2.41	89.78 ± 0.36
FE_{H2} (%)	20.30 ± 3.51	0.81 ± 0.27
Conversion (%)	79.07 ± 2.13	53.43 ± 6.65
S_{AP} (%)	89.75 ± 2.41	92.72 ± 0.47
TOF_{AP} (h^{-1})	10.35 ± 0.13	7.51 ± 0.90

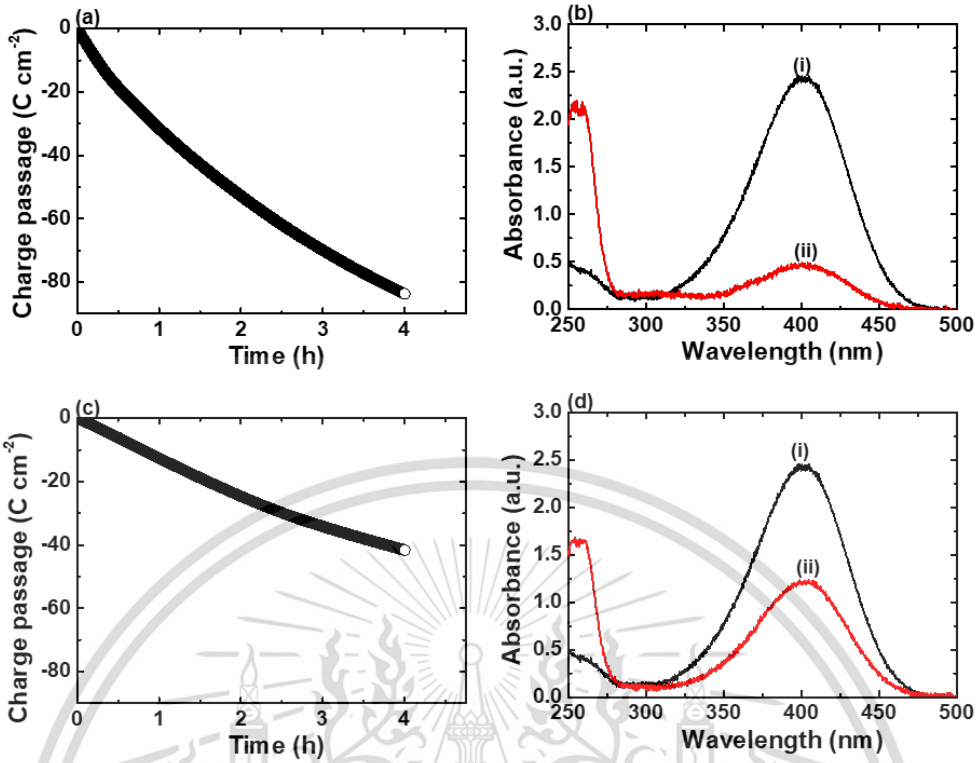

Figure 4-8 (a and c) Charge transients obtained from 4-h CPEs at -0.15 V vs. RHE with various electrode species in phosphate solution (0.5 M, pH 7) containing 4-NP (4 mM) and (b and d) UV-vis spectra of the as-prepared catholyte solution (i) and catholyte solutions obtained after 4-h CPEs (ii); (a-b) the *micro*NiP|CP electrode and (c-d) the *micro*FeP|CP electrode

4.2 Influence of pH values on *e*-NPR with *micro*NiFeP|CP electrode

For electrochemical properties of electrode, pH of electrolyte is considered parameter to finding the appropriate environment condition [20]; on the other hand, the electrochemical activity of the *micro*NiFeP|CP electrodes was influenced by pH values (5.0, 7.0, and 9.0), as displayed in **Figure 4-6**. Moreover, the pH of solution was also influenced of on formation of 4-NP and stability of 4-AP (as discussed in **Appendix A-1**). Therefore, the *micro*NiFeP|CP (r_{NiFe} = 0.5) electrode, which was prepared in the electrolyte containing–ammonium chloride (0.25 M), hypophosphite (1 M), nickel chloride (0.067 M), and ferrous sulfate (0.133 M) at I_{dep} of -20 mA cm^{-2} for 27 s, was considered in electrolytes with various pH values toward HER and *e*-NPR. The *micro*NiFeP|CP (r_{NiFe} = 0.5) electrode achieved the activity of HER and *e*-NPR in electrolytes of various pH values, as shown in LSV results (**Figure 4-6**). For HER

activities, the *micro*NiFeP|CP (r_{NiFe} = 0.5) electrode proposed the lowest onset and highest activity at pH 7.0, which displayed the $\eta_{10,HER}$ (-181.5 mV vs. RHE) was about 1.26 and 2.14 times higher than at pH 5.0 (-228.1 mV vs. RHE) and at pH 9.0 (-388.0 mV vs. RHE). The pH of electrolyses influences the reduction currents of e-NPR, a -64.8 mV vs. RHE of $\eta_{10,NPR}$ was achieved when electrolysis was performed under pH 7, which is about 2.67 and 2.46 times higher than electrolysis under pH 5.0 (-173.2 mV vs. RHE) and pH 9.0 (-159.2 mV vs. RHE), respectively; in other words, the reduction current first increased up to pH 7.0 and then started decreasing with further increases in pH. This phenomenon is probably explained based on electrostatic interaction, as with the increase in pH of the test solution, the electrode surface became more negative, which in turn repelled the negatively charged 4-NP and thus reduced its availability at the electrode surface [9, 16, 44].

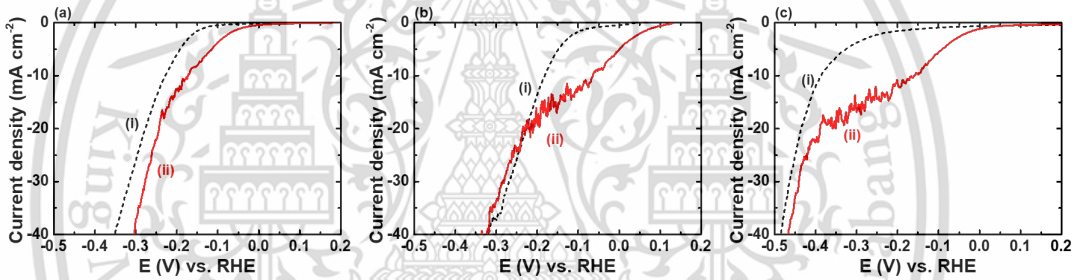

Figure 4-9 LSV of *micro*NiFeP|CP (r_{NiFe} = 0.5) electrode at various pH ((a) pH 5.0, (b) pH 7.0, and (c) pH 9.0) without (i) and with 4 mM of 4-NP (ii); Scan rate 10 mA s^{-1}.

To clearly understand the influence of pH values on e-NPR, the *micro*NiFeP|CP (r_{NiFe} = 0.5) electrode was investigated by a series of 1-h CPEs (at 0.10, 0.05, 0.00, -0.10, and -0.15 V vs. RHE) in various pH values (5.0, 7.0, and 9.0) and the enhancement of FE_{AP}, 4-NP conversion, selectivity of 4-AP, and TOF_{AP} with decreasing applied potential regardless of solution pH (from 0.10 V vs. RHE to -0.15 V vs. RHE) were shown in **Figure 4-10**. FE_{AP} (**Figure 4-10a**) exhibited excellent activities in all pH values. Specifically, pH 7.0 proposed the increasing of FE_{AP} from 83.42 ± 1.67% to 94.10 ± 2.84%; whereas pH 5.0 and pH 9.0 also found the increasing of FE_{AP} from 83.42 ± 1.67% to 94.10 ± 2.84% and from 83.42 ± 1.67% to 94.10 ± 2.84%, respectively, within decreased working potentials from 0.1 to -0.15 V vs. RHE. The *micro*NiFeP|CP (r_{NiFe} = 0.5) electrode exhibited significant increases in conversion of 4-NP (**Figure 4-10b**) and selectivity of 4-AP (**Figure 4-10c**) with decreasing applied

potential regardless of solution pH from 0.10 V vs. RHE to -0.15 V vs. RHE, especially pH 7.0 (1.36 ± 0.32% to 29.02 ± 0.70% and 37.07 ± 4.88% to 95.31 ± 3.99%, respectively). The e-NPR performance of the microNiFeP (r_{NiFe} = 0.5) electrode at pH 7.0 resulted excellent on TOF_{AP} (**Figure 4-10d**) which proposed significantly enhance from 0.32 ± 0.06 h^{-1} to 18.46 ± 1.11 h^{-1} with decreased working potentials from 0.10 V vs. RHE to -0.15 V vs. RHE. The findings of this study indicate that the process of *e*-NPR is unlikely to have occurred by electrocatalytic hydrogenation, specifically utilizing the Volmer reaction for the creation of adsorbed hydrogen atoms. In contrast, the proposed e-NPR mechanism involves an initial phase of direct electron transfer occurring between the *micro*NiFeP|CP (r_{NiFe} = 0.5) electrode and 4-NP. This is subsequently followed by further protonation processes taking place inside the aqueous electrolyte solution. The production of 4-AP from *e*-NPR necessitates a series of six hydrogen-coupled electron transfer reactions, potentially leading to the creation of 4-nitrosophenol and 4-hydroxyaminophenol as intermediate products.

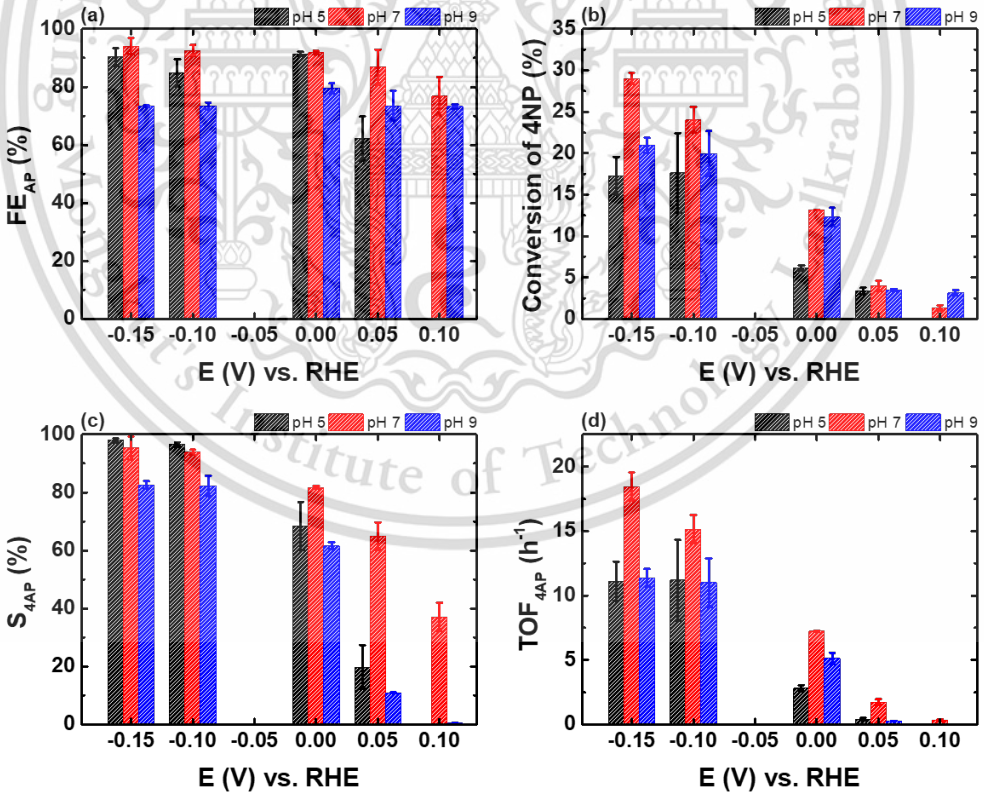

Figure 4-10 (a) FE_{AP}; (b) conversion of 4-NP; (c) Selectivity of 4-AP; and (d) TOF_{AP} of e-NPR 1 h by the *micro*NiFeP|CP (r=0.5) electrode in 0.5 M PBS containing 4 mM of 4-NP various pH values (pH 5.0 (black box); pH 7.0 (red box); and pH 9.0 (blue box)).

As discussed above and shown in **Figure 4-10**, the partial current densites or current densites responsible (J_{total}, J_{4AP}, and J_{Other}) at different working potentials at various pH values were eliminated and shown in **Figure 4-11**. All experiment results various pH proposed a significantly enhanced the partial current densites with decreaed working potential from 0.10 V vs. RHE to -0.15 V vs. RHE; espectially, the partial current densities at pH 7.0 (**Figure 4-11b**) resulted in a significant enhanced J_{total} (-0.15 $\pm$ 0.02 mA cm^{-2} to -6.83 $\pm$ 0.24 mA cm^{-2}), J_{4AP} (-0.11 $\pm$ 0.02 to -6.44 $\pm$ 0.39 mA cm^{-2}), and J_{Other} (-0.00 $\pm$ 0.00 mA cm^{-2} to -0.39 $\pm$ 0.18 mA cm^{-2}). Meanwhile, the comparison of pH influences at -0.15 V vs. RHE resulted in excellent *e*-NPR activity (J_{4AP}) at pH 7 (-6.44 $\pm$ 0.39 mA cm^{-2}) higher than at pH 5.0 (-3.88 $\pm$ 0.53 mA cm^{-2}) and at pH 9.0 (-3.98 $\pm$ 0.24 mA cm^{-2}). However, the partial current densites of other products (J_{Other}) displayed the highest incresing at pH 9.0 when decreased working potentials from 0.1 to -0.15 V vs. RHE (0.00 $\pm$ 0.00 mA cm^{-2} to -1.52 $\pm$ 0.03 mA cm^{-2}, respectively).

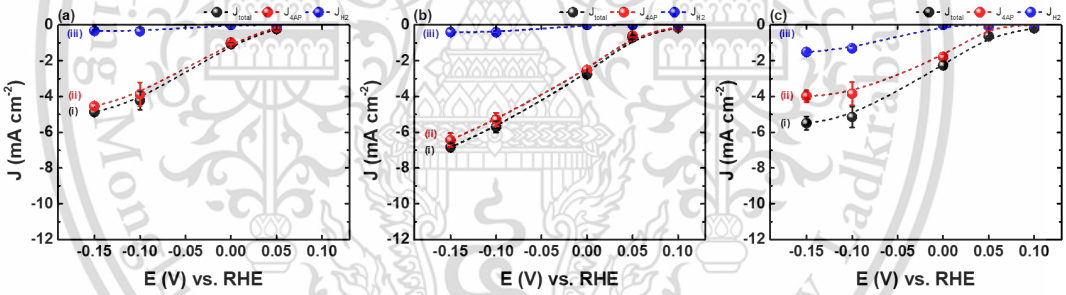

Figure 4-11 Current responsible (i: J_{total}, ii: J_{4AP}; and iii: J_{Other}) at various pH (a) pH 5.0; (b) pH 7.0; and (c) pH 9.0 with *micro*NiFeP|CP (r_{NiFe} = 0.5) electrodes

As revealed from **Figure 4-9** to **Figure 4-11**, the observed decrease in FE_{AP} and S_{AP} values at pH 9 can be attributed to several factors. Firstly, at potentials equal to or less than -0.1 V vs. RHE, the phenomenon of HER may contributes to this decrease. Additionally, the incomplete reduction of 4-NP could also play a role in reducing the FE_{AP} and S_{AP} values. Furthermore, there are side reactions occurring between the intermediates and 4-AP that contribute to this decrease. These side reactions include: (i) the reaction between p-benzoquinone imine, which is formed through the dehydration and structural rearrangement of 4-hydroxyaminophenol, and 4-AP to 4-Amino-3-[(4-hydroxyphenyl)amino]phenol at pH values greater than 8 [58]; (ii) the

condensation reaction between 4-nitrosophenol and 4-hydroxyaminophenol, resulting in the formation of 4,4'-dihydroxyazoxybenzene [59]; and (iii) the electrochemical reduction of 4,4'-dihydroxyazoxybenzene, which involves an additional two-electron transfer, leading to the formation of 4,4'-dihydroxyazobenzene [59]. However, it is possible to reduce the occurrence of side reactions by employing electrolyte solutions that possess lower pHs.

4.3 Influence of working potential and kinetic constants

4.3.1 Influence of working potential

As discussed in **sections 4.1** and **4.2**, the working potential was an important parameter toward *e*-NPR. To confirm the electrocatalytic performance and the positive shift of potential in LSV results (**Figure 4-5** and **Figure 4-9**) of the *micro*NiFeP|CP (r_{NiFe} = 0.5) electrode, *e*-NPR at pH 7.0 within 4-h CPEs at various working potentials (0.10 V vs. RHE to -0.20 V vs. RHE) was further investigated as shown in **Figure 4-12** and **Figure 4-13**. J_{total} (**Figure 4-13a**) and conversion of 4-NP (**Figure 4-13b**) increased from -0.153 ± 0.017 mA cm^{-2} to -5.079 ± 0.131 mA cm^{-2} and 3.45 ± 0.49% to 72.34 ± 0.82%, respectively, when the potential decreased from 0.10 V vs. RHE to -0.20 V vs. RHE. This means the working potential is an important factor for electrocatalytic reactions, indicating that the reductive current and conversion increase as the potential decreases [56, 60]. Meanwhile, S_{AP} (**Figure 4-13b**) significantly increased about 1.96 times (from 49% to 96%) at positive working potential ($E_{work} \geq 0.00$ V vs. RHE) and remained slightly stable about 96% at more negative potentials ($E_{work} < 0.00$ V vs. RHE). As revealed by J_{4AP} and J_{H2} in **Figure 4-13a**, indicating increased total current density as working potential decreased could facilitate e-NPR and HER [20]. In **Figure 4-13c**, the investigating 4-h CPEs at 0.00 V vs. RHE and -0.15 V vs. RHE could achieved 95.31 ± 1.73% and 97.37 ± 0.79% of FE_{AP}, respectively; however, 4-h CPEs at -0.20 V achieved only 80.54 ± 2.30% of FE_{AP}. While FE_{H2} increased from 0% to ~20% as working potential decreased from 0.00 V vs. RHE to -0.20 V vs. RHE, implying the competitive of HER and e-NPR at more negative working potential (< -0.20 V vs. RHE) [20]. Based on the abovementioned results, indicating working potentials were divided in 2 zones [8, 9, 61]. Under Zone I (at $E_{work} \geq 0.00$ V vs. RHE), that exhibited the reduction of 4-NP as the main reaction; while Zone II ($E_{work} < 0.00$ V vs. RHE), that exhibited the reduction of 4-NP and generation of hydrogen bubble on electrocatalyst surface at working potential decreased lower than 0.00 V vs RHE [9,

61]. Those indicates that the competitive of HER and e-NPR were decreasing working potential more than 0 V vs. RHE that relating to LSV results in **Figure 4-5**; however, the decreasing of working potential were beneficial on e-NPR which demonstrates in **Figure 4-13**. According to the demonstration above, the findings indicate that electrocatalytic hydrogenation of *e*-NPR is improbable to occur via the Volmer reaction, which is responsible for the generation of adsorbed hydrogen atoms. In contrast, the proposed *e*-NPR mechanism involves the first occurrence of direct electron transfer between the *micro*NiFeP|CP (r_{NiFe} = 0.5) electrode and 4-NP, afterwards followed by protonation processes within the aqueous electrolyte solution. While the working potential shown an impact on the selectivity of *e*-NPR and HER, all working potentials displayed a similar trend in terms of the electron transfer number for the reduction of 4-NP (n_{NPR}), which was about 6 (see **Figure 4-13d).** The production of 4-AP from *e*-NPR necessitates a series of six hydrogen-coupled electron transfer reactions, potentially leading to the creation of 4-nitrosophenol and 4-hydroxyaminophenol as intermediate products (**Figure 2-2**).

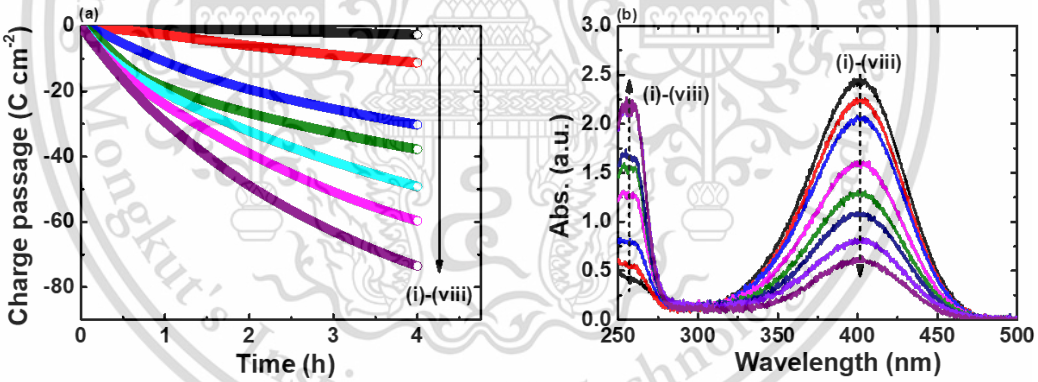

Figure 4-12 (a) Charge transients obtained from 4-h CPEs and (b) UV-vis spectra of the as-prepared catholyte solution the as-prepared catholyte solution (i) and catholyte solutions obtained after 4-h CPEs at various applied potentials (ii: 0.10 V vs. RHE; iii: 0.05 V vs. RHE; iv: 0.00 V vs. RHE; v: -0.05 V vs. RHE; vi: -0.10 V vs. RHE; vii: -0.15 V vs. RHE; viii: -0.20 V vs. RHE) in phosphate solution (0.5 M, pH 7) containing 4-NP (4 mM).

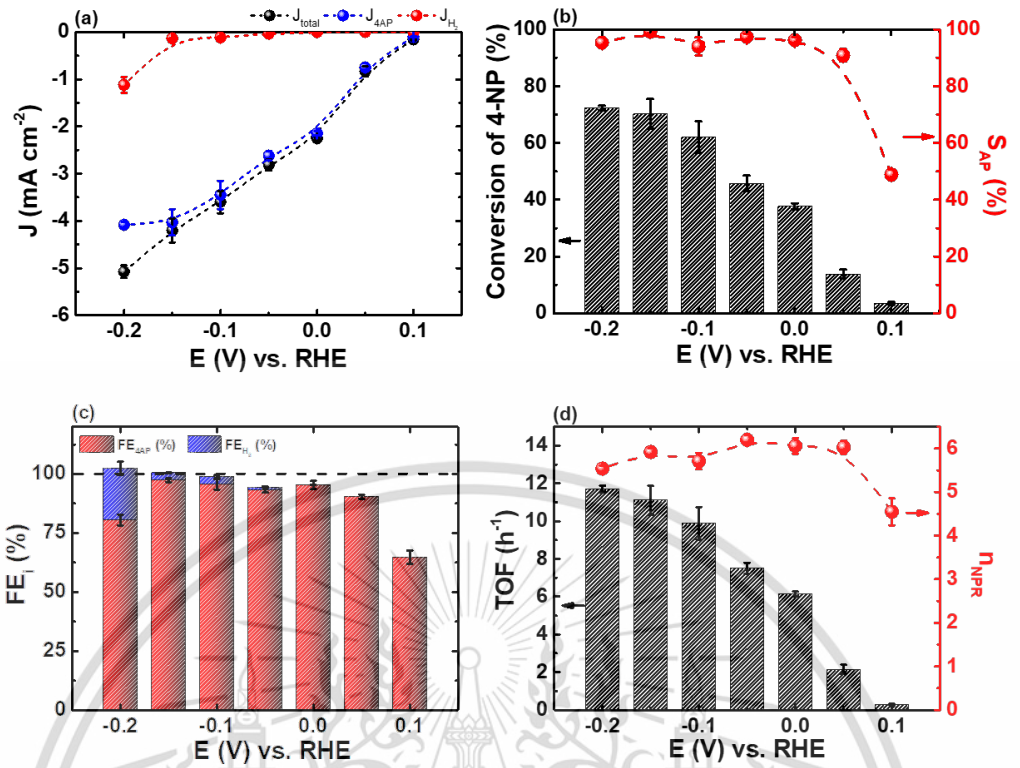

Figure 4-13 *e*-NPR various working potentials by 4-h CPEs of the *micro*NiFeP|CP (r_{NiFe} = 0.5) electrode in 0.5 M PBS (pH 7.0) containing 4 mM of 4-NP: (a) Total current (J_{total}), current responsible of HER (J_{H2}) and e-NPR (J_{NPR}); (b) Conversion of 4-NP and S_{AP}; (c) %FE of H_2 and 4-NP; and (d) TOF and n_{NPR}

The positive shift in potential observed in the linear sweep voltammetry (LSV) results, along with the significantly higher 4-nitrophenol (4-NP) conversion efficiency at 0.00 V vs. RHE compared to that at 0.10 V vs. RHE, can be attributed to enhanced electrostatic attraction facilitated by electrochemical assistance, as previously reported [25, 56, 62]. These findings are indicative of an additional redox reaction occurring between 4-NP and the metallic metal species, specifically Ni^0 and Fe^0, within the *micro*NiFeP|CP (r_{NiFe} = 0.5) electrode. To confirm this, a chemical catalytic reduction of 4-NP was conducted after 4 hours using the *micro*NiFeP|CP (r_{NiFe} = 0.5) electrodes, as shown in **Figure 4-14**. In this experiment, the *micro*NiFeP|CP (r_{NiFe} = 0.5) electrode was immersed in a deaerated electrolyte containing 4-NP without applying any bias for 4 hours.

As a result, a relatively low conversion of 4-NP (1.86 ± 0.10%) was observed, determined by a decrease in the absorbance at λ= 400 nm (as shown in **Figure 4-14a**). Additionally, a small amount of 4-aminophenol (4-AP) was generated, but with a low

selectivity for 4-AP (S_{AP}) of 7.71 ± 0.61%. This outcome is likely due to the incomplete reduction of 4-NP, owing to the limited availability of reducing equivalents from the small amount of Ni^0 and Fe^0 species within the *micro*NiFeP|CP (r_{NiFe} = 0.5) electrode.

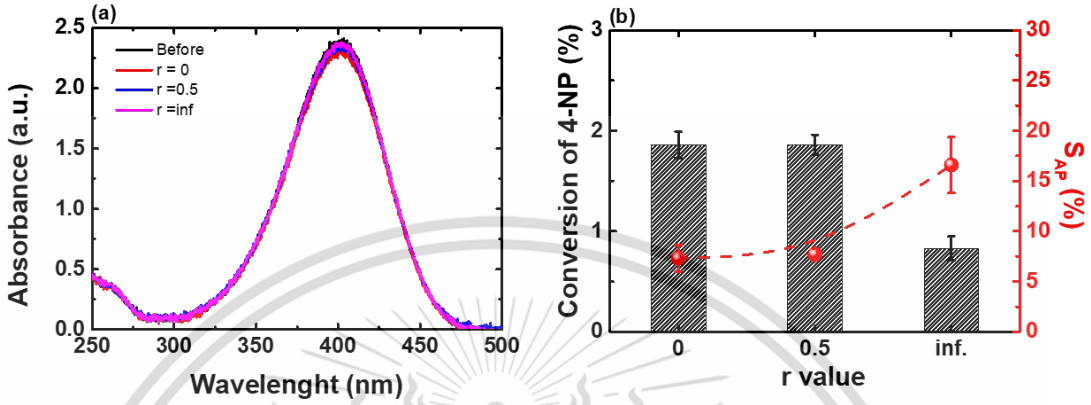

Figure 4-14 Chemical catalytic reduction of 4-NP after 4 h of the *micro*NiFeP|CP electrodes in PBS (0.5 M, pH 7.0) containing 4 mM of 4-NP without applying bias at room temperature: (a) UV-Vis spectrum of the catholyte solution before and after incubation; (b) Conversion of 4-NP and selectivity of 4-AP.

4.3.2 Rate constant toward e-NPR

To clearly understand the kinetics of electrochemical activity on the *e*-NPR of the *micro*NiFeP|CP (r_{NiFe} = 0.5) electrode, total charge passage (**Figure 4-15a**) was increased from 69.08 ± 2.51% to 96.22 ± 1.06% and from 86.51 ± 1.31% to 99.24 ± 0.55% when the electrolysis duration increased from 1 to 4 h at 0.00 V vs. RHE and -0.15 V vs. RHE, respectively. The conversion of 4-NP (**Figure 4-15c**) was increased from 69.08 ± 2.51% to 96.22 ± 1.06% and from 86.51 ± 1.31% to 99.24 ± 0.55% when the electrolysis duration increased from 1 to 4 h at 0.00 V vs. RHE and -0.15 V vs. RHE, respectively.

FE_{AP} (**Figure 4-15b**) was found to slightly increase from 76.25 ± 3.39% to 95.31 ± 1.73% and from 84.11 ± 2.82% to 97.37 ± 0.79% when the electrolysis duration increased from 1 to 4 h whereas those decreased to 84.82 ± 1.98% and 76.07 ± 7.20% when the electrolysis duration increased to 8 h at 0.00 V vs. RHE and -0.15 V vs. RHE, respectively.

Furthermore, S_{AP} (**Figure 4-15c**) was also found to slightly increase from 69.08 ± 2.51% to 96.22 ± 1.06% and from 86.51 ± 1.31% to 99.24 ± 0.55% when the

electrolysis duration increased from 1 to 4 h whereas those decreased to 87.83 ± 3.71% and 82.22 ± 3.88% when the electrolysis duration increased to 8 h at 0.00 V vs. RHE and -0.15 V vs. RHE, respectively.

The results suggest that side reactions probably competed with *e*-NPR throughout the prolonged electrolysis and transformation of 4-AP, which can be observed in the molar fraction (**Figure 4-16**) and stability of 4-AP in each solution recorded by HPLC analysis (**Figure A-3**). Moreover, it is probably that the amount of chemically adsorbed 4-NP on the surface of the cathode is limited by the amount of adsorption corresponding to the completion of a monolayer [19].

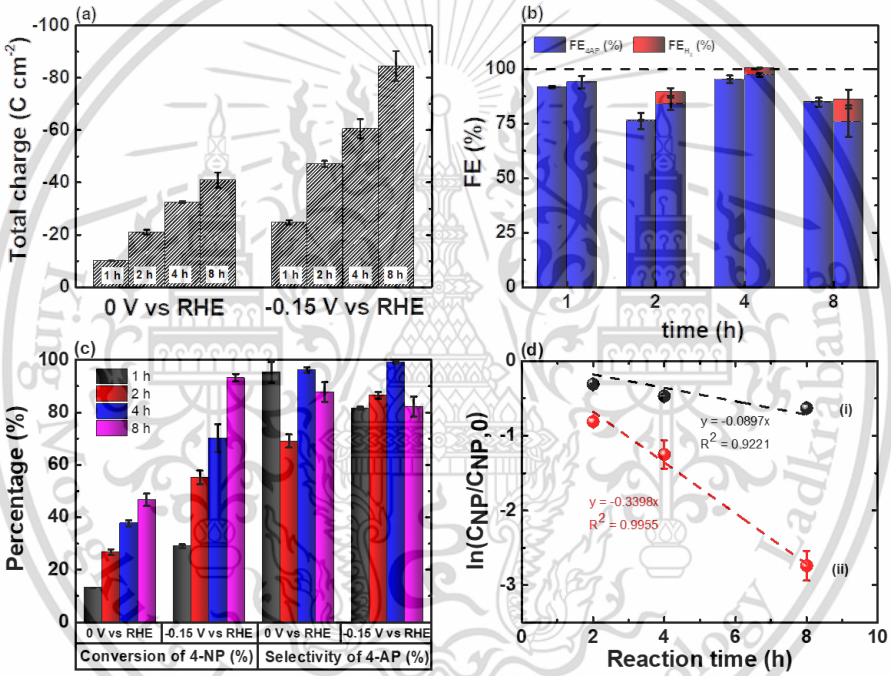

Figure 4-15 (a) Total charge passage; (b) FE of 4-AP and H_2; (c) Conversion of 4-NP and S_{AP}; and (d) plot of $\ln(C_{4NP}/C_{4NP,0})$ and time at -0.15 V vs. RHE

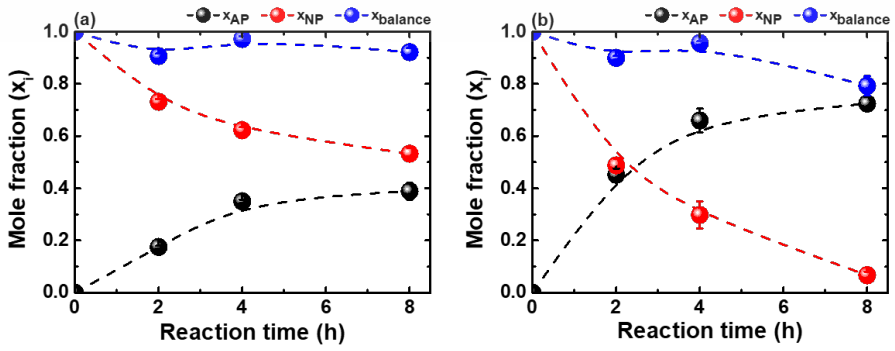

Figure 4-16 Mole fraction of *e*-NPR: (a) 0.00 V vs. RHE; and (b) -0.15 V vs. RHE

Furthermore, the apparent reaction rate constant (k) derived with a pseudo-first-order reaction model, as shown below Eq. **4-1**:

$$ln\left(\frac{C_{4NP}}{C_{4NP,0}}\right) = -kt \quad \textbf{(4-1)}$$

where $C_{4AP,0}$ is initial concentration of 4-NP, t is reaction time, and C_{4AP} is remaining concentration of 4-NP at t. **Figure 4-15d,** the figure demonstrates the relationship between $\ln(C_{4NP}/C_{4NP,0})$ and time, revealing a consistent increase in the apparent kinetic constants of *e*-NPR as the potential lowers at 0 V vs. RHE and -0.15 V vs. RHE on the *micro*NiFeP|CP (r_{NiFE} = 0.5) electrode [9, 56]. The study revealed that the observed kinetic constants were 0.091 h^{-1} cm^{-2} and 0.340 h^{-1} cm^{-2} for electrode-Nernstian potential ratio (*e*-NPR) values of 0 V vs. reversible hydrogen electrode (RHE) and -0.15 V vs. RHE, respectively. The electrocatalytic efficiency of the *micro*NiFeP|CP (r_{NiFe} = 0.5) electrode was evaluated and compared to the electrocatalysts documented in prior literature (**Table 4-3**). The performance index, namely the *e*-NPR rate, was used for comparison since it is shown that the conversion of 4-NP is significantly influenced by the concentration of 4-NP in the electrolysis [9, 20]. The *micro*NiFeP|CP (r_{NiFe} = 0.5) electrode has been shown to exhibit significant activity, positioning it as one of the highly active electrocatalysts documented in the existing literature [20]. In addition, the electrochemical characteristics, selectivity of *e*-NPR [16, 44], synthesis of 4-NP (**Figure A-1**) [22] and stability of 4-AP (**Figure A-3**) are influenced by the pH of the electrolyte.

Table 4-3 Comparison on electrocatalytic performant of modified *micro*NiFeP|CP electrode with those reported in the public literature.

Electrocatalyst	Electrolyte	The best condition						Ref.
		System	Applied potential (V vs. RHE)	Highest conversion (%)	Selectivity of 4-AP (%)	FE_{AP} (%)	Kinetic constant (h^{-1})	
TiO_2 with exposed [001] facets and oxygen vacancy	0.1 M NaCl containing 0.1 mM 4-NP (pH 5)	H-cell	-0.66	~100% after 2 h	89.70%	N.A.[b]	~0.1[c]	[9]
Mesoporous CoPt nanowires	1.0 M H_2SO_4 containing 0.7 mM 4-NP	H-cell	~ -0.15	~100% after 24 min	N.A.[b]	N.A.[b]	N.A.[b]	[63]
Carbon black supported Mn-MIL-100 framework	0.25 M NaCl containing 0.7 mM 4-NP (pH 2)	H-cell	-0.591	96% after 12 h	76%	N.A.[b]	N.A.[b]	[64]
Porous Au micropillars	0.4 M Na_2SO_4 containing 5 mM 4-NP (pH 2)	H-cell	-0.072	99% after 3 h	N.A.[b]	N.A.[b]	0.03[d]	[65]
Pt nanoparticles	0.5 M H_2SO_4 containing 33.2 mM 4-NP	H-cell	-0.023	83.1% after 12 h	N.A.[b]	9.90%	N.A.[b]	[66]

Table 4-3 Comparison on electrocatalytic performant of modified *micro*NiFeP|CP electrode with those reported in the public literature. (Cont.)

Electrocatalyst	Electrolyte	The best condition						Ref.
		System	Applied potential (V vs. RHE)	Highest conversion (%)	Selectivity of 4-AP (%)	FE_{AP} (%)	Kinetic constant (h^{-1})	
Silver and gold	0.1 M Na_2SO_4 containing 5.25 mm 4-NP (pH 2)	H-cell	-0.25 (Ag) -0.15 (Au)	> 80% after 150 min	N.A.[b]	N.A.[b]	0.070 (Ag) 0.084 (Au)	[61]
Single sheet iron(III) hydroxides	0.05 M HEPES containing 100 µM 3-NP (pH 7)	H-cell	~0.1	74.5% after 330 min	37.80%	39.90%	0.1299	[44]
microNiFeP_{op} (r = 2, 0.2 M $H_2PO_2^-$)	0.5 M PBS containing 4 mM 4-NP (pH 7)	H-cell	-0.2	89.6 ± 3.3% after 8 h	73.66%	81.98%	0.291	[20]
$CuCo_2O_4$/nickel foam	1.0 M KOH containing 20 mM	H-cell	~ -0.2	~92% after 300 C passage	97.20%	89%	N.A.	[8]
NiB_x/nickel foam	1.0 M KOH containing 10 mM 4-NP	H-cell	0	~100% after 50 min	~100%	99%	N.A.	[7]
Ru-PA/NF	1 M KOH containing 5 mM 4-NP	H-cell	-0.67	94.7% after 9 h	99%	73.20%	0.306	[67]

Table 4-3 Comparison on electrocatalytic performant of modified *micro*NiFeP|CP electrode with those reported in the public literature. (Cont.)

Electrocatalyst	Electrolyte	The best condition						Ref.
		System	Applied potential (V vs. RHE)	Highest conversion (%)	Selectivity of 4-AP (%)	FE_{AP} (%)	Kinetic constant (h^{-1})	
CF-Cu(OH)$_2$	1.0 M KOH cantaining 10 mM 4-NP and 0.1 M $NaBH_4$	H-cell	~-0.1	~100% after 3 h (224 C passage)	95.50%	98.70%	N.A.	[48]
Ni-MOF/NF	0.1 M KOH containing 0.5 mM 4-NP	H-cell	~-0.034	91.2% after 6 h	N.A.	N.A.	~0.042 (h^{-1} mg^{-1})	[47]
Ag/Ni–MOF	1 M KOH containing 25 mM 4-NP	H-cell	~ 0.17	98.4% after 5 h	~100%	99.80%	~0.808	[45]
CeO_2/Ni-MOF	1 M KOH containing 25 mM 4-NP	H-cell	−0.9 V vs Hg/HgO	97.6% after 6 h (565.7 C)	100%	99.90%	N.A.[b]	[46]
*micro*NiFeP|CP_{op}	0.5 M PBS containing 4 mM 4-NP (pH 7)	H-cell	-0.15	70.25 ± 5.20 % after 4 h	93.97 ± 0.52%	92.21 ± 0.74%	0.33	*This work*
*micro*NiFeP|CP_{op}	0.5 M PBS containing 10 mM 4-NP (pH 7)	Flow-type electrolyzer	-10 mA cm^{-2}	68.52 ± 0.69 % after 1 h	91.9 ± 0.61%	77.30 ± 0.38%	0.8716	*This work*

4.4 Circulation flow-system electrolyzer

Circulation flow-system was utilized to improve performance and solve the limit of mass transfer toward *e*-NPR [68]. *e*-NPR involves proton transfer; consequently, prolonged electrolysis would result in a significant rise in pH within the concentration boundary layer of the batch system. This significant increase in pH would activate secondary reactions, resulting in a decrease in S_{AP}. On the other hand, the high 4-NP conversion in the prolonged electrolysis at moderate applied potentials (-0.1 -0.2 V vs. RHE) in the batch system would decrease the bulk 4-NP concentration and thus reduce the concentration gradient, resulting in the decreased availability of 4-NP, the low mass-transfer rate of 4-NP, and the competition of HER. To counteract these mass-transfer-induced negative effects, a flow-type electrochemical electrolyzer (**Figure 3-3**) was designed and implemented for constant-current electrolysis.

4.4.1 Influence of current for e-NPR

Figure 4-17 shown the influence of applied current density toward *e*-NPR. The partial current the competitive of e-NPR and HER as shown in **Figure 4-17b.** Moreover, the FE_{AP} decreased when increasing current density, that indicates the competitiveness was enhanced with increasing current density.

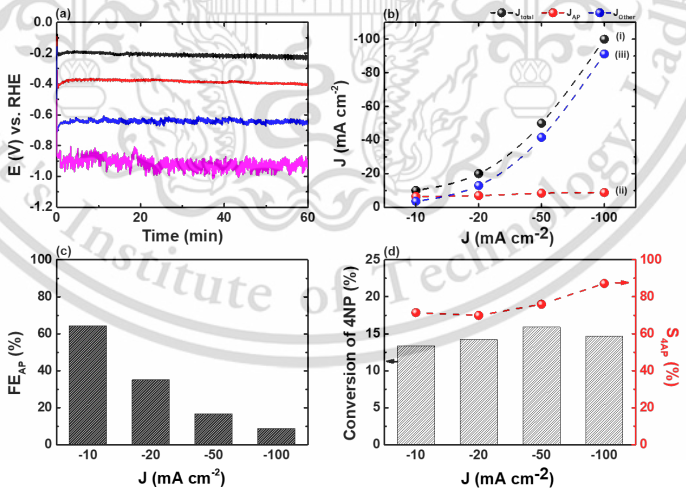

Figure 4-17 Cyclic flow-system toward *e*-NPR with various CCEs (-10, -20, -50, and -100 mA cm^{-2}) with 95% iR compensation by the *micro*NiFeP|CP (r_{NiFe} = 0.5) electrode (1 cm^{-2}) in 0.5 M PBS (pH 7.0) containing 4 mM of 4-NP: (a) Chronopotentiometric curves (P-t); (b) Partial current (i: J_{total}, ii: J_{4AP}; and iii: J_{other}); (c) FE_{AP}; and (d) Conversion of 4-NP and S_{AP}.

4.4.2 Scale up electrode surface and electrolyzer size

The data depicted in **Figure 4-18** illustrate the outcomes derived from the constant-current electrolysis conducted using a flow-type electrolyzer operating at a current density of -10 mA cm^{-2}. This electrolysis was performed in a phosphate solution with a concentration of 0.5 M and a pH value of 7, which also contained 4-NP at a concentration of 10 mM. The results indicate that the *micro*NiFeP|CP (r_{NiFe} = 0.5) electrode had significantly superior performance when used in the flow-type electrochemical electrolyzer compared to the 8-hour prolonged batch electrolysis, as shown in **Figure 4-15**. Significantly, the utilization of a flow-type electrolyzer in the process of electrolysis yielded a higher conversion rate of 4-NP (93.84 ± 0.84% compared to 92.29 ± 1.47%) and a higher reaction rate of reduction of 4-nitrophenol (21.18 ± 0.28 μmole cm^{-2} h^{-1} compared to 14.13 ± 0.10 μmole cm^{-2} h^{-1}) with a selectivity towards the desired product (86.32 ± 1.05%) within a shorter time frame (specifically, 3 hours), even when exposed to a higher initial concentration of 4-NP (10 mM compared to 4 mM).

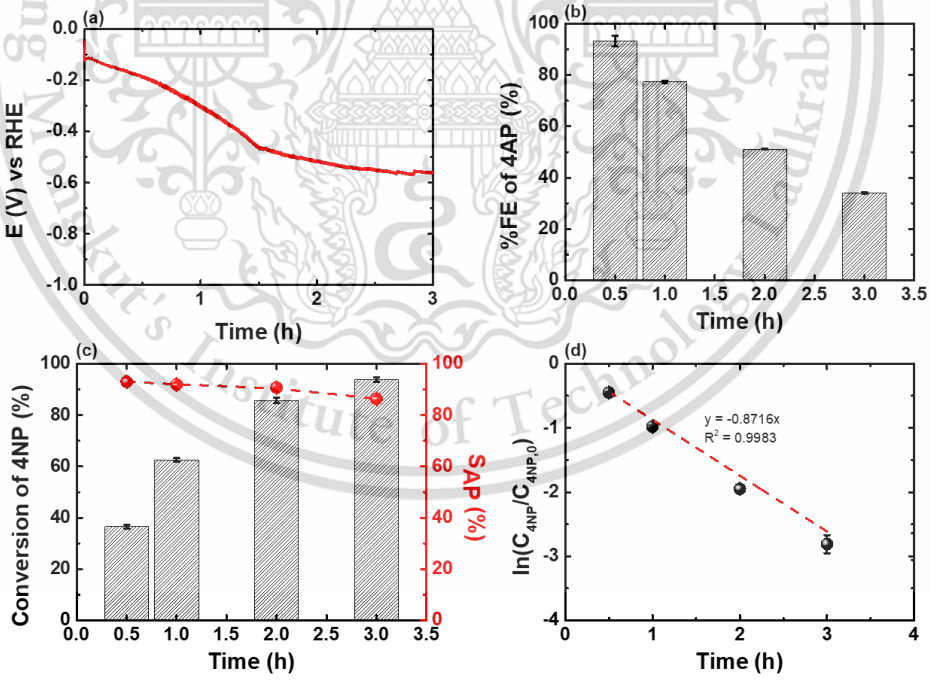

Figure 4-18 Cyclic flow-system toward *e*-NPR with various CCEs at -10mA cm^{-2} with 95% iR compensation by the *micro*NiFeP|CP_{op} electrode (1 cm^{-2}) in 0.5 M PBS (pH 7.0) containing 4 mM of 4-NP: (a) Chronopotentiometric curves (P-t); (d) Partial current (i: J_{total}, ii: J_{4AP}; and iii: J_{other}); (c) %FE of 4-AP; and (d) Conversion of 4-NP and selectivity of 4-AP.

Furthermore, the utilization of a flow-type electrolyzer in the electrolysis process resulted in a rate constant of 0.95 h^{-1}, as seen in **Figure 4-18**. This value is about 2.8 times greater than the rate constant of 0.34 h^{-1} achieved in the batch electrolysis experiment, where a similar conversion of 4-NP was observed (**Figure 4-18**). It should be noted that a consistent rise in potential and a decline in Faradaic efficiency for the anodic oxidation of 4-NP were observed during the process of electrolysis. This phenomenon can be attributed to the lower concentration of 4-NP in the bulk solution at higher conversion rates, which restricts the attainment of the maximum limiting current and facilitates the occurrence of other undesired electrochemical reactions, such as the hydrogen evolution reaction (HER).

In contrast to a batch-system, it is noteworthy that the utilization of a 3-CCEs method utilizing the H-cell at a current density of -10 mA cm^{-2} in a PBS (0.5 M, pH 7) containing 4-NP (10 mM), as depicted in **Figure 4-19**, yielded comparable conversion (97.95 ± 0.51%) and reaction rate per unit area (R_{AP} = 25.18 ± 0.22 μmole cm^{-2} h^{-1}). However, this approach necessitated a higher overpotential (0.05 ~ 0.2 V) in comparison to the utilization of a flow-type electrolyzer.

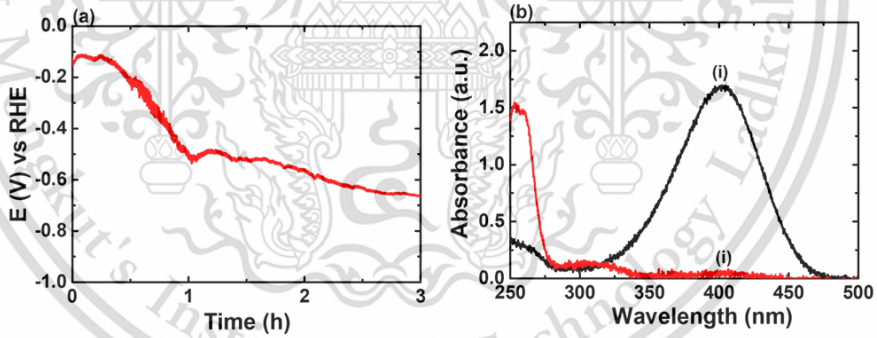

Figure 4-19 (a) Potential-transient recorded from constant-current electrolysis at -10 mA cm^{-2} using a H-cell (batch electrolysis) in 4-AP (10 mM)-containing phosphate solution (0.5 M, pH 7). (b) UV-vis spectra of the as-prepared catholyte solution (i) and catholyte solution obtained after 3-h CCEs at -10 mA cm^{-2}.

4.5 Mechanism of *e*-NPR with *micro*NiFeP|CP

The mechanism of e-NPR was briefly investigated with the cyclic voltammetry (CV) was performed in 3 cycles with a potential window of 1 to -0.5 V vs. RHE at various scanning rates of 10, 50, 100, 200, and 250 mV s^{-1} to briefly investigate

e-NPR's phenomena on *micro*NiFeP|CP, as shown in **Figure 4-20**. CV shown in **Figure 4-20** illustrated that the character oxidation and reduction peak. In detail, there is no obvious current until the potential trigger HER in PBS, nevertheless, the pronounced redox couple (O_1/R_1) and reduction peak (R_2) present with the additional of 4 mM 4-NP, as shown in **Figure 4-20c [**18**]**.

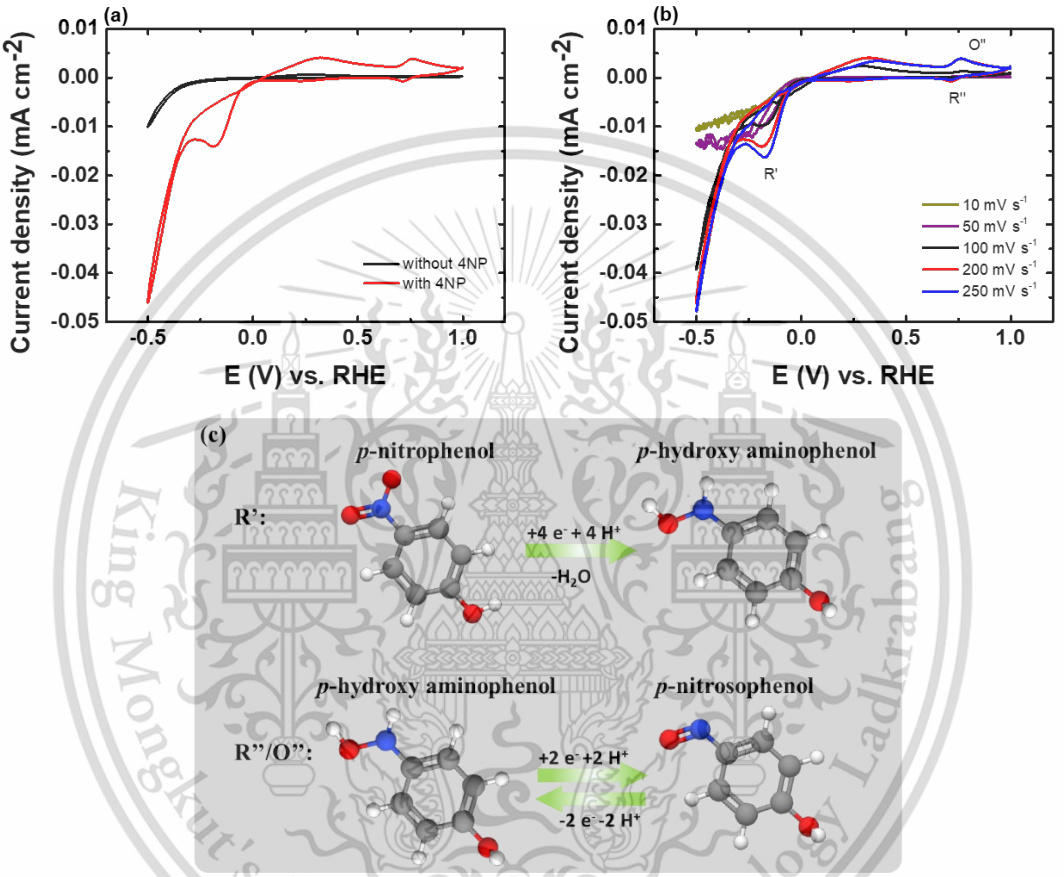

Figure 4-20 Cyclic Voltammetry of *micro*NiFeP|CP at neutral pH (a) at 250 mV s^{-1} ((i) without and (ii) with 4 mM 4-NP); (b) with 4 mM 4-NP at various scan rates (10, 50, 100, 200, 250 mV s^{-1}); and (c) Redox reaction of e-NPR

In order to get a thorough comprehension of the underlying mechanism involved in the *e*-NPR, liquid chromatography-mass spectrometry (LC-MS) analysis subsequent to the electrolysis process was performed. The outcomes of this research are depicted in **Figure 4-21**. In addition to the detection of 4-aminophenol (with a strong peak observed at m/z of 110.06 Da), the analysis also revealed the presence of various intermediates and side products. These include p-benzoquinone imine (with a peak observed at m/z of 108.04 Da), semi-quinoneimine radical derivative (with m/z of

109.05 Da), 4,4'-Dihydroxyazobenzene (with a peak observed at m/z of 215.08 Da), (3-[(4-Hydroxyphenyl)amino]-4-imino-2,5-cyclohexadien-1-one) (with a peak observed at m/z of 215.12 Da), and 4-Amino-3-[(4-hydroxyphenyl)amino]phenol (with a peak observed at m/z of 217.2 Da). The emergence of these byproducts provides insight into the factors contributing to the divergence of the selectivity for 4-aminophenol (S_{AP}) from complete (100%) selectivity.

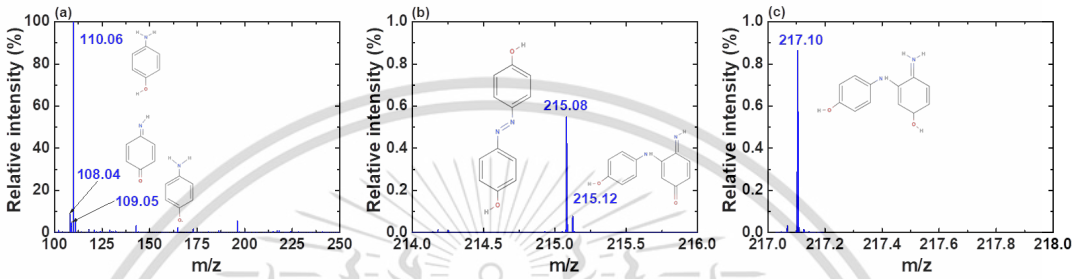

Figure 4-21 The LCMS results of e-NPR products: (a) m/z 100 to 250; (b) m/z 214 to 216; and (c) m/z 217 to 218

As the above discussion (in **Figure 4-21**), these findings led to the development of a proposed reaction pathway for e-NPR at the *micro*NiFeP|CP electrode, as illustrated in **Figure 4-22**. The pathway involves the formation of two dimers: (3-[(4-Hydroxyphenyl)amino]-4-imino-2,5-cyclohexadien-1-one) and 4-Amino-3-[(4-hydroxyphenyl)amino]phenol, which are generated through a reaction with p-benzoquinone imine. This p-benzoquinone imine is produced via the dehydration and structural rearrangement of 4-hydroxyaminophenol (representing side reaction A). Additionally, 4,4'-dihydroxyazobenzene is formed through the condensation reaction between 4-nitrosophenol and 4-hydroxyaminophenol, representing side reaction B.

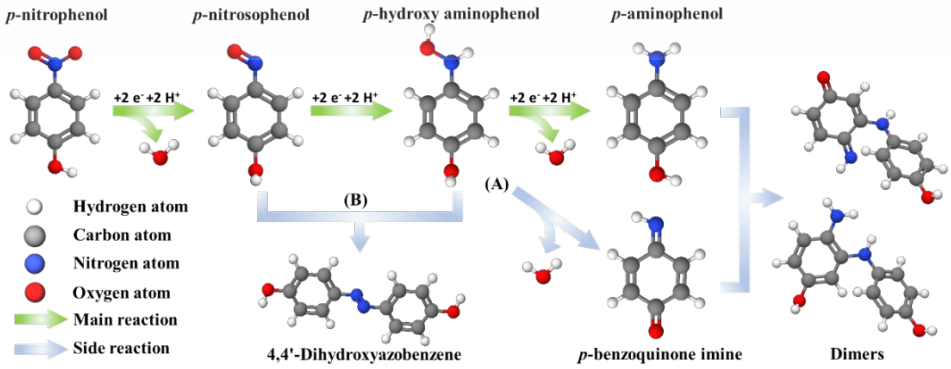

Figure 4-22 Reaction pathway of e-NPR with *micro*NiFeP|CP in neutral pH

CHAPTER 5
CONCLUSION

5.1 Conclusions

The electrodeposition process for *micro*NiFeP|CP electrode was further optimized to investigate the kinetics of 4-nitrophenol (4-NP) electroreduction on the developed *micro*NiFeP|CP_{OP} electrode (as r_{NiFe} = 0.5) under circumneutral pH conditions in the present study. The resulting *micro*NiFeP|CP_{OP} electrode primarily consisted of metallic iron, metallic nickel, and nickel phosphide. Only a small quantity of 4-aminophenol (4-AP) was produced through a redox reaction involving 4-NP and the metallic metal species (Ni^0 and Fe^0) within the *micro*NiFeP|CP_{OP} electrode. Electrochemical hydrogenation via the Volmer reaction pathway was unlikely for *e*-NPR. Instead, the process was initiated by direct electron transfer between the *micro*NiFeP|CP_{OP} electrode and 4-NP, followed by protonation steps in the aqueous electrolyte. Successful scale-up electrosynthesis of 4-AP using a flow-type electrolyzer was also demonstrated. The formation of dimers and 4,4'-dihydroxyazobenzene side products during electrolysis accounted for the deviation from 100% selectivity, confirming the presence of two primary side reaction pathways.

5.2 Suggestions

As shown in the above results, the *micro*NiFeP|CP proposed the activity of *e*-NPR at high HER's potential but low selectivity, as shown in **Figure 4-5**, **Figure 4-9**, and **Figure 5-1**. To mitigate the competitiveness of HER occurring at potentials above HER's potential (higher than 0 V vs. RHE), the photo-electrochemical reduction of 4-NP *(Photo)e*-NPR is possible to enhance the reducibility of 4-NP and improving its selectivity over the HER [14, 37, 42].

Photo-electrochemical reduction involves utilizing light energy to drive electrochemical reactions, potentially offering a way to control the reduction of 4-NP selectively. This method could be explored to alter the reaction pathway and favor the reduction of 4-NP over the competing HER at lower potentials. The combination of *micro*NiFeP|CP with a photo-electrochemical reduction strategy may offer a pathway to improve the selectivity of 4-NP reduction, potentially addressing the issue of low selectivity observed in the *micro*NiFeP|CP system at high potential.

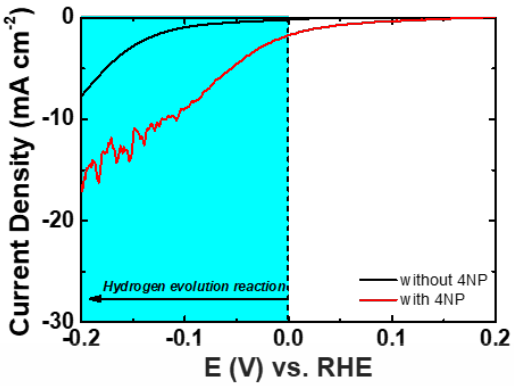

Figure 5-1 LSV of *micro*NiFeP|CP (r_{NiFe} = 0.5) electrode without (i) and with 4 mM of 4-NP (ii); Scan rate 10 mA s^{-1}.

Additionally, copper bismuth oxide (CBO; $CuBi_2O_4$|FTO) proves intriguing for optimizing photo-electrochemical reduction and hydrogen generation [37] as shown in **Figure 5-2**.

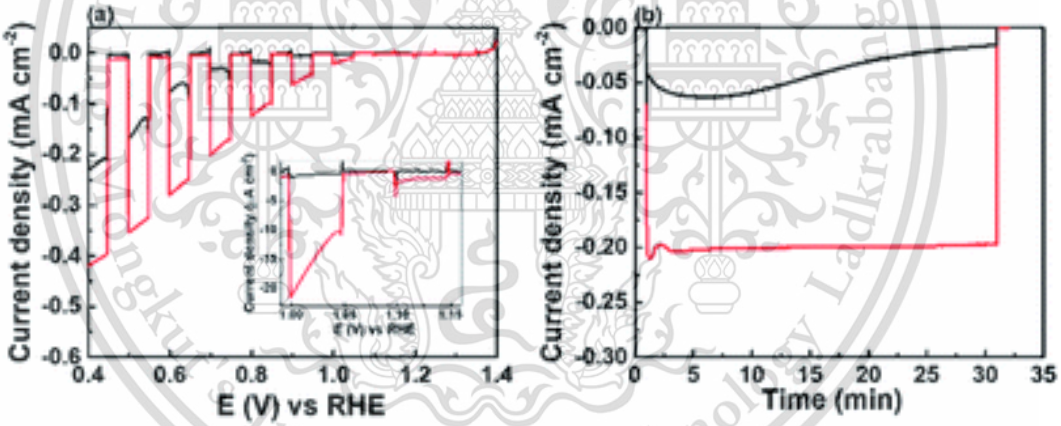

Figure 5-2 (a) Typical linear sweep voltammograms, recorded at a scan rate of 10 mV s^{-1}, of nano$CuBi_2O_4$ in NaOH solution (0.1 M) under chopped light illumination under N_2 (black trace) and O_2 (red trace) atmospheres. (b) Photocurrent transient behaviour of nano$CuBi_2O_4$ at 0.7 V vs. RHE in NaOH solution (0.1 M) under N_2 (black trace) and O_2 (red trace) atmospheres. [37]

$CuBi_2O_4$|FTO is possible to be the alternative electrocatalytic toward the reduction of 4-NP. **Figure 5-3** shows the enhancement of activity toward *(Photo)e*-NPR.

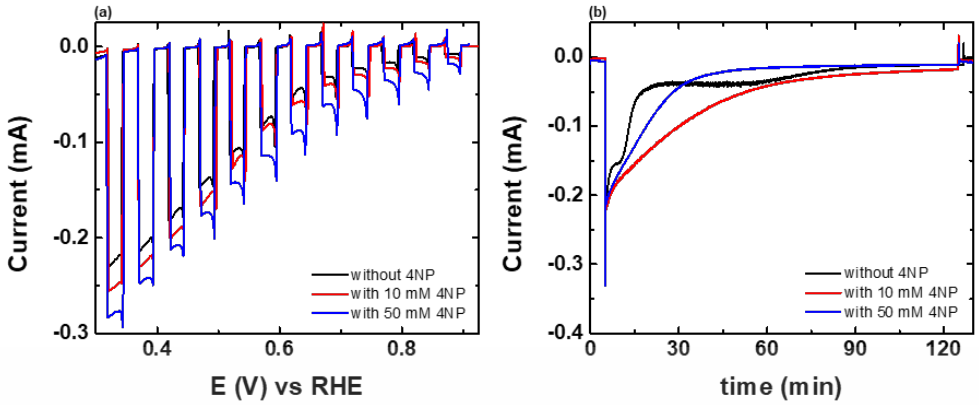

Figure 5-3 (a) LSV, recorded at a scan rate of 10 mV s^{-1}, of $CuBi_2O_4$|FTO in various concentrations of 4-NP; (b) Photocurrent transient behavior at 0.35 V vs. RHE.

REFERENCES

[1] R. P. Pohanish, "N," in *Sittig's Handbook of Toxic and Hazardous Chemicals and Carcinogens (Sixth Edition)*, R. P. Pohanish Ed. Oxford: William Andrew Publishing, 2012, pp. 1894-2017.

[2] J. Strachan, C. Barnett, A. F. Masters, and T. Maschmeyer, "4-Nitrophenol Reduction: Probing the Putative Mechanism of the Model Reaction," (in English), *Acs Catal,* vol. 10, no. 10, pp. 5516-5521, May 15 2020, doi: 10.1021/acscatal.0c00725.

[3] Y. M. Magdy, H. Altaher, and E. ElQada, "Removal of three nitrophenols from aqueous solutions by adsorption onto char ash: equilibrium and kinetic modeling," (in English), *Appl Water Sci,* vol. 8, no. 1, Mar 2018, doi: 10.1007/s13201-018-0666-1.

[4] X. T. Zhan, S. Michaud-Chevallier, D. Herault, and F. Duprat, "On-Line Analysis of the Heterogeneous Pd-Catalyzed Transfer Hydrogenation of p-Nitrophenol in Water with Formic Acid in a Flow Reactor," (in English), *Org Process Res Dev,* vol. 24, no. 5, pp. 686-694, May 15 2020, doi: 10.1021/acs.oprd.9b00291.

[5] L. Y. Zeng *et al.*, "Neutral-pH overall water splitting catalyzed efficiently by a hollow and porous structured ternary nickel sulfoselenide electrocatalyst," (in English), *J Mater Chem A,* vol. 7, no. 28, pp. 16793-16802, Jul 28 2019, doi: 10.1039/c9ta05601g.

[6] S. H. Yuan, M. Tian, Y. P. Cui, L. Lin, and X. H. Lu, "Treatment of nitrophenols by cathode reduction and electro-Fenton methods," (in English), *J Hazard Mater,* vol. 137, no. 1, pp. 573-580, Sep 1 2006, doi: 10.1016/j.jhazmat.2006.02.069.

[7] P. L. Zhang *et al.*, "Paired Electrocatalytic Oxygenation and Hydrogenation of Organic Substrates with Water as the Oxygen and Hydrogen Source," (in English), *Angew Chem Int Edit,* vol. 58, no. 27, pp. 9155-9159, Jul 1 2019, doi: 10.1002/anie.201903936.

[8] S. T. Wu, X. Huang, H. L. Zhang, Z. D. Wei, and M. Wang, "Efficient Electrochemical Hydrogenation of Nitroaromatics into Arylamines on a

CuCo2O4 Spinel Cathode in an Alkaline Electrolyte," (in English), *Acs Catal,* vol. 12, no. 1, pp. 58-65, Jan 7 2022, doi: 10.1021/acscatal.1c03763.

[9] C. C. Ni *et al.*, "Synergistic role of electron-trapped oxygen vacancy and exposed TiO2 [001] facets toward electrochemical p-nitrophenol reduction: Characterization, performance and mechanism," (in English), *Chemical Engineering Journal,* vol. 411, May 1 2021, doi: 10.1016/j.cej.2021.128485.

[10] M. Jin *et al.*, "Selective electrocatalytic hydrogenation of nitrobenzene over copper-platinum alloying catalysts: Experimental and theoretical studies," (in English), *Appl Catal B-Environ,* vol. 298, Dec 5 2021, doi: 10.1016/j.apcatb.2021.120545.

[11] L. Lerner, "Identity of a purple dye formed by peroxidic oxidation of p-aminophenol at low pH," *J Phys Chem A,* vol. 115, no. 35, pp. 9901-10, Sep 8 2011, doi: 10.1021/jp2045806.

[12] G. Scandurra, A. Antonella, C. Ciofi, G. Saitta, and M. Lanza, "Electrochemical detection of p-aminophenol by flexible devices based on multi-wall carbon nanotubes dispersed in electrochemically modified Nafion," *Sensors (Basel),* vol. 14, no. 5, pp. 8926-39, May 21 2014, doi: 10.3390/s140508926.

[13] S. C. Mitchell, P. Carmichael, and R. Waring, "Aminophenols," in *Kirk-Othmer Encyclopedia of Chemical Technology*, vol. 2, 2000, pp. 652-678.

[14] C. Y. Lin, S. C. Huang, Y. G. Lin, L. C. Hsu, and C. T. Yi, "Electrosynthesized Ni-P nanospheres with high activity and selectivity towards photoelectrochemical plastics reforming," (in English), *Appl Catal B-Environ,* vol. 296, Nov 5 2021, doi: 10.1016/j.apcatb.2021.120351.

[15] S. C. Huang, C. C. Cheng, Y. H. Lai, and C. Y. Lin, "Sustainable and selective formic acid production from photoelectrochemical methanol reforming at near-neutral pH using nanoporous nickel-iron oxyhydroxide-borate as the electrocatalyst," *Chemical Engineering Journal,* vol. 395, Sep 2020, Art no. 125176, doi: 10.1016/j.cej.2020.125176.

[16] Renu *et al.*, "Unfolding the electrocatalytic efficacy of highly conducting NiFe2O4-rGO nanocomposites on the road to rapid and sensitive detection of hazardous p-Nitrophenol," (in English), *J Electroanal Chem,* vol. 887, Apr 15 2021, doi: 10.1016/j.jelechem.2021.115161.

[17] A. F. Baye, D.-H. Han, S. K. Kassahun, R. Appiah-Ntiamoah, and H. Kim, "Improving the reduction and sensing capability of Fe3O4 towards 4-

nitrophenol by coupling with ZnO/Fe0/Fe3C/graphitic carbon using ZnFe-LDH@carbon as a template," *Electrochimica Acta,* vol. 398, p. 139343, 2021/12/01/ 2021, doi: 10.1016/j.electacta.2021.139343.

[18] S. Chinnapaiyan *et al.*, "Ultrasonic-assisted preparation and characterization of magnetic ZnFe2O4/g-C3N4 nanomaterial and their applications towards electrocatalytic reduction of 4-nitrophenol," (in English), *Ultrason Sonochem,* vol. 68, Nov 2020, doi: 10.1016/j.ultsonch.2020.105071.

[19] T. C. Pereira, E. F. Zanoelo, F. H. Passig, C. Beninca, and K. Q. de Carvalho, "Reduction of p-nitrophenol in an airlift electrochemical reactor with iron electrodes," (in English), *J Environ Chem Eng,* vol. 9, no. 3, Jun 2021, doi: 10.1016/j.jece.2021.105223.

[20] S. C. Huang, Z. X. You, S. M. Jhang, and C. Y. Lin, "Facile electrochemical preparation of NiFeP submicron-spheres as an efficient electrocatalyst for the electrochemical hydrogenation of 4-nitro-phenol at neutral pH," (in English), *J Environ Chem Eng,* vol. 10, no. 6, Dec 2022, doi: 10.1016/j.jece.2022.108882.

[21] Agency for Toxic Substances and Disease Registry (ATSDR), *Toxicological Profile for Nitrophenols (Draft for Public Comment)*. Atlanta: GA: U.S. Department of Health and Human Services, Public Health Service, 2022.

[22] M. Ayan-Varela *et al.*, "Achieving extremely concentrated aqueous dispersions of graphene flakes and catalytically efficient graphene-metal nanoparticle hybrids with flavin mononucleotide as a high-performance stabilizer," *ACS Appl Mater Interfaces,* vol. 7, no. 19, pp. 10293-307, May 20 2015, doi: 10.1021/acsami.5b00910.

[23] J. Li, C.-y. Liu, and Y. Liu, "Au/graphene hydrogel: synthesis, characterization and its use for catalytic reduction of 4-nitrophenol," *Journal of Materials Chemistry,* vol. 22, no. 17, pp. 8426-8430, 2012, doi: 10.1039/C2JM16386A.

[24] R. P. Pohanish, "N," in *Sittig's Handbook of Toxic and Hazardous Chemicals and Carcinogens (Seventh Edition)*, R. P. Pohanish Ed.: William Andrew Publishing, 2017, pp. 2291-2438.

[25] M. F. Wu, Y. N. Jin, G. H. Zhao, M. F. Li, and D. M. Li, "Electrosorption-promoted Photodegradation of Opaque Wastewater on A Novel TiO2/Carbon Aerogel Electrode," (in English), *Environ Sci Technol,* vol. 44, no. 5, pp. 1780-1785, Mar 1 2010, doi: 10.1021/es903201m.

[26] L. R. Sassykova *et al.*, "Studying the Mechanisms of Nitro Compounds Reduction (A-Review)," (in English), *Orient J Chem,* vol. 35, no. 1, pp. 22-38, 2019, doi: 10.13005/ojc/350103.

[27] M. T. Shah *et al.*, "SiO2 caped Fe3O4 nanostructures as an active heterogeneous catalyst for 4-nitrophenol reduction," (in English), *Microsyst Technol,* vol. 23, no. 12, pp. 5745-5758, Dec 2017, doi: 10.1007/s00542-017-3431-8.

[28] S. Gopi and K. Yun, "Cerium-iron phosphate nano flower bifunctional electrocatalyst for efficient electrochemical detection and catalytic reduction of hazardous 4-nitrophenol," (in English), *J Environ Chem Eng,* vol. 10, no. 6, Dec 2022, doi: 10.1016/j.jece.2022.108938.

[29] X. K. Kong, H. Y. Zhu, C. L. Chen, G. M. Huang, and Q. W. Chen, "Insights into the reduction of 4-nitrophenol to 4-aminophenol on catalysts," (in English), *Chem Phys Lett,* vol. 684, pp. 148-152, Sep 16 2017, doi: 10.1016/j.cplett.2017.06.049.

[30] J. C. de Souza, B. F. da Silva, D. A. Morales, G. D. Umbuzeiro, and M. V. B. Zanoni, "Assessment of p-aminophenol oxidation by simulating the process of hair dyeing and occurrence in hair salon wastewater and drinking water from treatment plant," (in English), *J Hazard Mater,* vol. 387, Apr 5 2020, doi: 10.1016/j.jhazmat.2019.122000.

[31] M. Durovic, J. Hnat, and K. Bouzek, "Electrocatalysts for the hydrogen evolution reaction in alkaline and neutral media. A comparative review," (in English), *J Power Sources,* vol. 493, May 1 2021, doi: 10.1016/j.jpowsour.2021.229708.

[32] X. Xu, X. M. Tian, Z. Zhong, L. T. Kang, and J. N. Yao, "In-situ growth of iron/nickel phosphides hybrid on nickel foam as bifunctional electrocatalyst for overall water splitting," (in English), *J Power Sources,* vol. 424, pp. 42-51, Jun 1 2019, doi: 10.1016/j.jpowsour.2019.03.084.

[33] J. M. Wang, Z. Liu, Y. W. Zheng, L. Cui, W. R. Yang, and J. Q. Liu, "Recent advances in cobalt phosphide based materials for energy-related applications," (in English), *J Mater Chem A,* vol. 5, no. 44, pp. 22913-22932, Nov 28 2017, doi: 10.1039/c7ta08386f.

[34] J. Y. Liu *et al.*, "Breaking the scaling relations of oxygen evolution reaction on amorphous NiFeP nanostructures with enhanced activity for overall seawater

splitting," (in English), *Appl Catal B-Environ,* vol. 302, Mar 2022, doi: 10.1016/j.apcatb.2021.120862.

[35] D. Sharma, P. Choudhary, S. Kumar, and V. Krishnan, "Transition Metal Phosphide Nanoarchitectonics for Versatile Organic Catalysis," (in English), *Small,* vol. 19, no. 11, Mar 2023, doi: 10.1002/smll.202207053.

[36] Y. L. Gu, F. Guo, Y. T. Qian, H. G. Zheng, and Z. P. Yang, "A solvothermal synthesis of ultra-fine iron phosphide," (in English), *Mater Res Bull,* vol. 37, no. 6, pp. 1101-1105, May 2002. [Online]. Available: <Go to ISI>://WOS:000176902900009.

[37] C. Y. Lin, S. Y. Lin, M. C. Tsai, and C. H. Wu, "Facile room-temperature growth of nanostructured CuBi2O4 for selective electrochemical reforming and photoelectrochemical hydrogen evolution reactions," (in English), *Sustain Energ Fuels,* vol. 4, no. 2, pp. 625-632, Feb 1 2020, doi: 10.1039/c9se00558g.

[38] Y. K. Zhang and L. Song, "Structural Designs and in-situ X-ray Characterizations of Metal Phosphides for Electrocatalysis," (in English), *Chemcatchem,* vol. 12, no. 14, pp. 3621-3638, Jul 21 2020, doi: 10.1002/cctc.202000233.

[39] H. Ishikawa *et al.*, "Air-Stable and Reusable Cobalt Phosphide Nanoalloy Catalyst for Selective Hydrogenation of Furfural Derivatives," (in English), *Acs Catal,* vol. 11, no. 2, pp. 750-757, Jan 15 2021, doi: 10.1021/acscatal.0c03300.

[40] T. Y. Chen *et al.*, "Nanosheet self-assembled NiCoP microflowers as efficient bifunctional catalysts (HER and OER) in alkaline medium," (in English), *Int J Hydrogen Energ,* vol. 46, no. 58, pp. 29889-29895, Aug 23 2021, doi: 10.1016/j.ijhydene.2021.06.121.

[41] S. C. Perry, C. P. de León, and F. C. Walsh, "Review-The Design, Performance and Continuing Development of Electrochemical Reactors for Clean Electrosynthesis," (in English), *J Electrochem Soc,* vol. 167, no. 15, Dec 1 2020, doi: 10.1149/1945-7111/abc58e.

[42] A. Das, K. Panigrahi, and P. Howli, "Photoelectrochemistry-driven ambient nitrogen reduction to ammonia: Materials' design insights," (in English), *Catal Today,* vol. 423, Nov 1 2023, doi: 10.1016/j.cattod.2022.12.010.

[43] R. N. Nunez, J. M. Betancourth, P. I. Ortiz, and V. Pfaffen, "Voltammetric Quantification of 4-Nitrophenol Using a Multivariate Optimized Plated

Bismuth Film Electrode," (in English), *Ind Eng Chem Res,* vol. 58, no. 27, pp. 12411-12418, Jul 10 2019, doi: 10.1021/acs.iecr.9b01700.

[44] L. Z. Huang, H. C. B. Hansen, and M. J. Bjerrum, "Electrochemical reduction of nitroaromatic compounds by single sheet iron oxide coated electrodes," (in English), *J Hazard Mater,* vol. 306, pp. 175-183, Apr 5 2016, doi: 10.1016/j.jhazmat.2015.12.009.

[45] H. Q. Zhao *et al.*, "Ag/Ni-MOF heterostructure with synergistic enrichment and activation properties for electrocatalytic reduction of 4-nitrophenol," (in English), *Chem Commun,* vol. 58, no. 97, pp. 13499-13502, Dec 6 2022, doi: 10.1039/d2cc05374h.

[46] H. Q. Zhao, X. L. Pang, Y. F. Huang, C. Ma, H. Y. Bai, and W. Q. Fan, "CeO2/Ni-MOF with Synergistic Function of Enrichment and Activation: Efficient Reduction of 4-Nitrophenol Pollutant to 4-Aminophenol," (in English), *Inorg Chem,* vol. 61, no. 49, pp. 19806-19816, Dec 12 2022, doi: 10.1021/acs.inorgchem.2c02937.

[47] H. Q. Zhao *et al.*, "Electrocatalytic reduction of 4-nitrophenol over Ni-MOF/NF: understanding the self-enrichment effect of H-bonds," (in English), *Chem Commun,* vol. 58, no. 31, pp. 4897-4900, Apr 14 2022, doi: 10.1039/d2cc00111j.

[48] X. L. Pang, H. Y. Bai, H. Q. Zhao, W. Q. Fan, and W. D. Shi, "Efficient Electrocatalytic Oxidation of 5-Hydroxymethylfurfural Coupled with 4-Nitrophenol Hydrogenation in a Water System," (in English), *Acs Catal,* vol. 12, no. 2, pp. 1545-1557, Jan 21 2022, doi: 10.1021/acscatal.1c04880.

[49] C. Costentin, S. Drouet, M. Robert, and J. M. Saveant, "Turnover Numbers, Turnover Frequencies, and Overpotential in Molecular Catalysis of Electrochemical Reactions. Cyclic Voltammetry and Preparative-Scale Electrolysis," *Journal of the American Chemical Society,* vol. 134, no. 27, pp. 11235-11242, Jul 2012, doi: 10.1021/ja303560c.

[50] W. H. Chen, J. R. Zeng, G. W. Zhang, J. Yu, and Y. J. Qiu, "Electrodeposition of Mo-doped NiFex nanospheres on 3D graphene fibers for efficient overall alkaline water splitting," (in English), *Int J Hydrogen Energ,* vol. 47, no. 29, pp. 13850-13861, Apr 5 2022, doi: 10.1016/j.ijhydene.2022.02.144.

[51] W. Z. Xia *et al.*, "Magnetic Fe3O4@C nanoparticles separated from cold rolling mill sludge for 4-nitrophenol reduction," (in English), *Sep Purif Technol,* vol. 309, Mar 15 2023, doi: 10.1016/j.seppur.2022.123018.

[52] M. Yamashita, H. Miyuki, Y. Matsuda, H. Nagano, and T. Misawa, "THE LONG-TERM GROWTH OF THE PROTECTIVE RUST LAYER FORMED ON WEATHERING STEEL BY ATMOSPHERIC CORROSION DURING A QUARTER OF A CENTURY," *Corrosion Science,* vol. 36, no. 2, pp. 283-299, Feb 1994, doi: 10.1016/0010-938x(94)90158-9.

[53] I. Chourpa *et al.*, "Molecular composition of iron oxide nanoparticles, precursors for magnetic drug targeting, as characterized by confocal Raman microspectroscopy," *Analyst,* 10.1039/B419004A vol. 130, no. 10, pp. 1395-1403, 2005, doi: 10.1039/B419004A.

[54] A. E. Henkes, Y. Vasquez, and R. E. Schaak, "Converting Metals into Phosphides: A General Strategy for the Synthesis of Metal Phosphide Nanocrystals," *Journal of the American Chemical Society,* vol. 129, no. 7, pp. 1896-1897, 2007/02/01 2007, doi: 10.1021/ja0685021.

[55] X. H. Su and C. W. Qiang, "Influence of pH and bath composition on properties of Ni-Fe alloy films synthesized by electrodeposition," (in English), *B Mater Sci,* vol. 35, no. 2, pp. 183-189, Apr 2012, doi: 10.1007/s12034-012-0284-8.

[56] J. J. Ma, Z. M. Wang, T. Majima, and G. H. Zhao, "Role of Ni in PtNi Alloy for Modulating the Proton-Electron Transfer of Electrocatalytic Hydrogenation Revealed by the In Situ Raman-Rotating Disk Electrode Method," (in English), *Acs Catal,* vol. 12, no. 22, pp. 14062-14071, Nov 18 2022, doi: 10.1021/acscatal.2c03551.

[57] A. Z. Li, X. Zhao, Y. N. Hou, H. J. Liu, L. Y. Wu, and J. H. Qu, "The electrocatalytic dechlorination of chloroacetic acids at electrodeposited Pd/Fe-modified carbon paper electrode," (in English), *Appl Catal B-Environ,* vol. 111, pp. 628-635, Jan 12 2012, doi: 10.1016/j.apcatb.2011.11.016.

[58] K. C. Brown and J. F. Corbett, "Benzoquinone imines. Part 16. Oxidation of p-aminophenol in aqueous solution," *Journal of the Chemical Society, Perkin Transactions 2,* 10.1039/P29790000308 no. 3, pp. 308-311, 1979, doi: 10.1039/P29790000308.

[59] C. J. Liang, Y. T. Lin, and J. W. Shiu, "Reduction of nitrobenzene with alkaline ascorbic acid: Kinetics and pathways," *Journal of Hazardous Materials,* vol. 302, pp. 137-143, Jan 2016, doi: 10.1016/j.jhazmat.2015.09.029.

[60] M. Sun, D. D. Reible, G. V. Lowry, and K. B. Gregory, "Effect of Applied Voltage, Initial Concentration, and Natural Organic Matter on Sequential Reduction/Oxidation of Nitrobenzene by Graphite Electrodes," (in English), *Environ Sci Technol,* vol. 46, no. 11, pp. 6174-6181, Jun 5 2012, doi: 10.1021/es300048y.

[61] A. Serra, R. Artal, M. Pozo, J. Garcia-Amoros, and E. Gomez, "Simple Environmentally-Friendly Reduction of 4-Nitrophenol," (in English), *Catalysts,* vol. 10, no. 4, Apr 2020, doi: 10.3390/catal10040458.

[62] X. N. Li, S. Chen, X. Quan, and Y. B. Zhang, "Enhanced Adsorption of PFOA and PFOS on Multiwalled Carbon Nanotubes under Electrochemical Assistance," (in English), *Environ Sci Technol,* vol. 45, no. 19, pp. 8498-8505, Oct 1 2011, doi: 10.1021/es202026v.

[63] A. Serrà, X. Alcobé, J. Sort, J. Nogués, and E. Vallés, "Highly efficient electrochemical and chemical hydrogenation of 4-nitrophenol using recyclable narrow mesoporous magnetic CoPt nanowires," (in English), *J Mater Chem A,* vol. 4, no. 40, pp. 15676-15687, 2016, doi: 10.1039/c6ta07149j.

[64] D. Chen *et al.*, "Carbon black supported on a Mn-MIL-100 framework as high-efficiency electrocatalysts for nitrophenol reduction," (in English), *J Electroanal Chem,* vol. 903, Dec 15 2021, doi: 10.1016/j.jelechem.2021.115824.

[65] M. Tranchant *et al.*, "Efficient and green electrochemical synthesis of 4-aminophenol using porous Au micropillars," (in English), *Appl Catal a-Gen,* vol. 602, Jul 25 2020, doi: 10.1016/j.apcata.2020.117698.

[66] T. X. Wu, G. Z. Wang, Y. X. Zhang, S. H. Kang, and H. M. Zhang, "Electrochemical deposition of Pt on carbon fiber cloth utilizing Pt mesh counter electrode during hydrogen evolution reaction for electrocatalytic hydrogenation reduction of p-nitrophenol," (in English), *New J Chem,* vol. 41, no. 15, pp. 7012-7019, Aug 7 2017, doi: 10.1039/c7nj01438d.

[67] M. H. Liu, A. Q. Kong, J. L. Zhang, Y. Fu, and W. Li, "Phytic acid-assisted fabrication of superhydrophilic Ru 3D electrode for electrocatalytic

hydrogenation of p-Nitrophenol," (in English), *Int J Hydrogen Energ,* vol. 47, no. 4, pp. 2187-2199, Jan 12 2022, doi: 10.1016/j.ijhydene.2021.10.209.

[68] J. D. Egbert *et al.*, "Development and Scale-up of Continuous Electrocatalytic Hydrogenation of Functionalized Nitro Arenes, Nitriles, and Unsaturated Aldehydes," (in English), *Org Process Res Dev,* vol. 23, no. 9, pp. 1803-1812, Sep 2019, doi: 10.1021/acs.oprd.8b00379.

APPENDIX

Appendix A: Supplementary data

Formation of 4-NP and decay of 4-AP in electrolytes difference pH values

According to the public literature, electrochemical reduction of 4-NP showed excellent performance toward reduction of 4-NP in a wide range of pH values, especially strong acidic or strong alkaline; furthermore, electrochemical sensors for the detection of 4-NP were proposed to have a high activity and reduction current of 4-NP when operating at a pH close to neutral. The dependence of 4-NP form on the pH of the solution was considered. 4-NP was dissolved in 0.5 M PBS at various pH values: acidic (pH 5), neutral (pH 7), and alkaline (pH 9). The intense color of solutions depending on pH was observed, as shown by the fact that increasing pH values (pH 5 to 9) turned the color of the solution from slightly yellow to intense yellow, as shown in **Figure A-1a.** The UV-Vis absorption in **Figure A-1b** demonstrates that there are two absorption peaks at 316 and 400 nm, indicating that the pH of the electrolyte influences the formation of 4-NP. A strong absorption band at 316 nm indicates that 4-NP is completely protonated in acidic solution, and a strong absorption at 400 nm indicates that 4-NP is completely deprotonated into the 4-nitrophenol anion in alkaline solution. Meanwhile, 4-NP appears to have both absorption peaks in neutral solution due to the presence of both formations of 4-NP, which are related to the Henderson-Hasselbalch equation and acid dissociation (in **Figure A-1c**), as a fraction of deprotonated 4-NP increases with increasing pH values [22, 23].

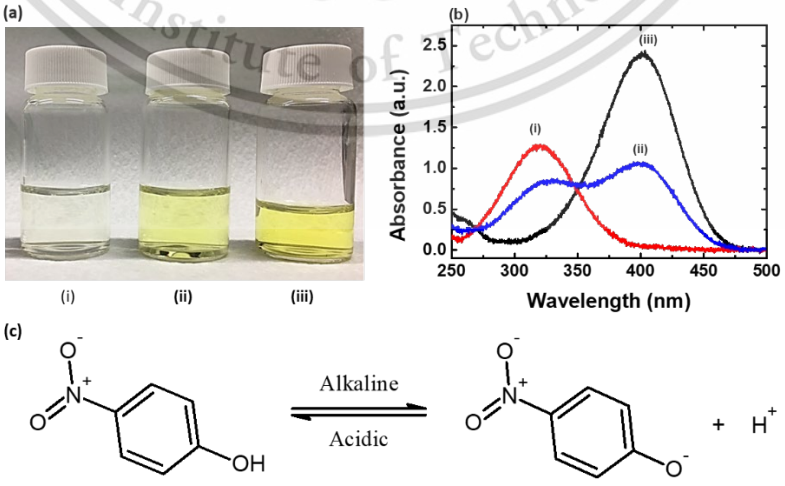

Figure A-0-1 (a) Digital photographs; (b) UV-Vis spectrum; and (c) acid dissociation equilibrium of 4-NP in PBS various pH values (i: pH 5; ii: pH 7; iii: pH 9).

Therefore, the determination of 4-NP concentration was measured and performed using a standard calibration curve in alkaline media to avoid the overlap absorption peak of products at 316 nm (such as 4-aminolphenol, benzoquinone, and hydroquinone) [2]. Additionally, 4-AP, the main product of e-NPR is easily oxidized by oxygen and light [13]. The 4-AP standard (4 mM) as standard solution for calibration curve was dissolved in deaerated PBS solutions (0.5 M; pH 7) with N_2 to degassed O_2 and avoid oxidation; however, there was also changed color and precipitated after incubation durations as shown in **Figure A-2**. HPLC of 4-AP was indicated the decay of 4-AP at incubation durations. Therefore, influence of pH on decay of 4-AP was investigated which was dissolved in deaerated solutions with N_2 including sodium sulfate (0.5 M; pH 2) and PBS (0.5 M; pH 7 and 12); the color of the solution turned from colorless to brown under neutral conditions and from slightly purple to dark purple under alkaline conditions, while there was no color change under acidic conditions.

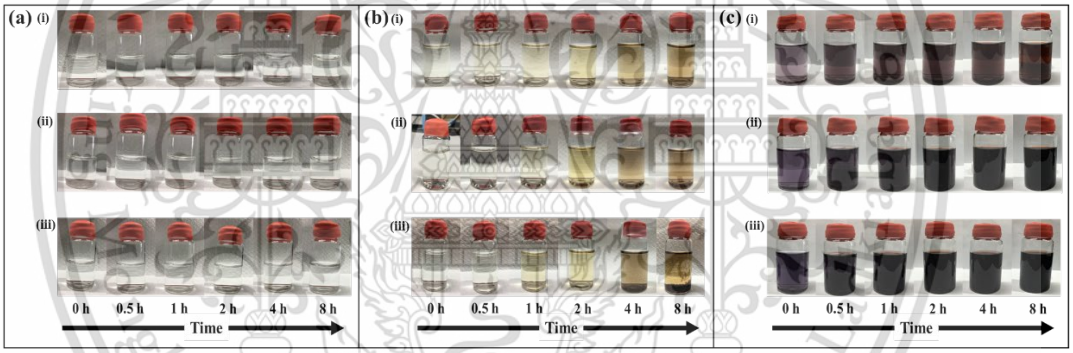

Figure A-0-2 Photographs at different incubation durations at various concentration of 4-AP (i: 0.5 mM; ii: 2 mM; and iii: 4 mM) and difference solutions: (a) 0.5 M H2SO4 (pH 2); (b) 0.5 M PBS (pH 7): and (c) 0.5 M PBS (pH 12)

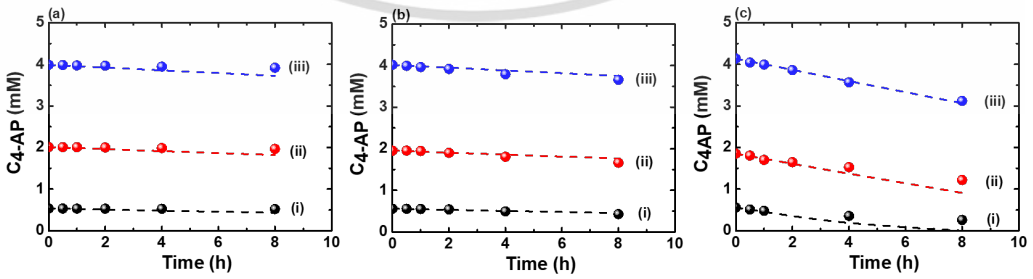

Figure A-0-3 The HPLC results various concentration of 4-AP (i: 0.5 mM; ii: 2 mM; and iii: 4 mM) in (b) 0.5 M H_2SO_4 (pH 2); (c) 0.5 M PBS (pH 7): and (d) 0.5 M PBS (pH 12)).

BIBLIOGRAPHY

Name: Papontee Sae Ong

Date of Birth: April 8, 1998

Address: 72 Rotphai Road, Sateng Sub- district, Mueang Yala, Yala, Thailand 95000

E-mail: Papontee.SO@hotmail.com, 63010793@kmitl.ac.th

Academic Background: 2020, Bachelor's Degree of Chemical Engineering, Department of Chemical Engineering, School of Engineering, King Mongkut' s Institute of Technology Ladkrabang

2023, Dual Mater's Degree of Chemical Engineering,

- Department of Chemical Engineering, School of Engineering, King Mongkut' s Institute of Technology Ladkrabang, Thailand
- Department of Chemical Engineering, Faculty of Engineering, National Cheng Kung University, Taiwan

Working Experience: 2019, process engineering internship in SCG Excellent Internship Program #18 at SCG ICO Polymers Co., Ltd.

Publication and award:

- Honorable Poster Award in 2023 Taiwan International Conference on Catalysis (TICC 2023), "Efficient and selective electrosynthesis of 4-aminophenol at neutral pH based on NiFeP electrode"
- Papontee Sae Ong, Shih-Ching Huang, Chia-Yu Lin, Nuttapol Lerkkasemsan, "Efficient and selective electrosynthesis of 4-aminophenol at circumneutral pH from the electrocatalytic reduction of nitrophenol over the nickel-iron phosphide modified electrode", Materials Today Sustainability, 2023, 100547, DOI: 10.1016/j.mtsust.2023.100547